Atmos. Chem. Phys. Discuss., 13, 15007–15059, 2013
www.atmos-chem-phys-discuss.net/13/15007/2013/
doi:10.5194/acpd-13-15007-2013

Atmospheric Chemistry and Physics Discussions

Comparison of MODIS 3 km and 10 km resolution aerosol optical depth retrievals over land with airborne sunphotometer measurements during ARCTAS summer 2008

J. M. Livingston[1], J. Redemann[2], Y. Shinozuka[3,4], R. Johnson[2], P. B. Russell[2], Q. Zhang[3,4], S. Mattoo[5,6], L. Remer[7], R. Levy[5], L. Munchak[5,6], and S. Ramachandran[8]

[1]SRI International, Menlo Park, California, USA
[2]NASA Ames Research Center, Moffett Field, California, USA
[3]NASA ARC-CREST, Moffett Field, California, USA
[4]Bay Area Environmental Research Institute, Sonoma, California, USA
[5]Earth Science Division, NASA Goddard Space Flight Center, Greenbelt, Maryland, USA
[6]Science Systems and Applications, Inc., Lanham, Maryland, USA
[7]Joint Center for Earth Systems Technology, University of Maryland, Baltimore County (JCET/UMBC), Baltimore, Maryland, USA
[8]Physical Research Laboratory, Ahmedabad, India

Received: 10 April 2013 – Accepted: 14 May 2013 – Published: 7 June 2013

Correspondence to: J. M. Livingston (john.livingston@sri.com)

Published by Copernicus Publications on behalf of the European Geosciences Union.

ACPD
13, 15007–15059, 2013

Abstract

Airborne sunphotometer measurements acquired by the NASA Ames Airborne Tracking Sunphotometer (AATS-14) from the NASA P-3 research aircraft are used to evaluate dark-target over-land retrievals of extinction aerosol optical depth (AOD) from spatially and temporally near-coincident measurements by the Moderate Resolution Imaging Spectroradiometer (MODIS) during the summer 2008 Arctic Research of the Composition of the Troposphere from Aircraft and Satellites (ARCTAS) field campaign. The new MODIS Collection 6 aerosol data set includes retrievals of AOD at both 10 km × 10 km and 3 km × 3 km (at nadir) resolution. In this paper we compare MODIS and AATS AOD at 553 nm in 58 10 km and 134 3 km retrieval grid cells. These AOD values were derived from data collected over Canada on four days during short time segments of five (four Aqua and one Terra) satellite overpasses of the P-3 during low altitude P-3 flight tracks. Three of the five MODIS/AATS coincidence events were dominated by smoke: one included a P-3 transect of a well-defined smoke plume in clear sky, but two were confounded by the presence of scattered clouds above smoke. The clouds limited the number of MODIS retrievals available for comparison, and led to MODIS AOD retrievals that underestimated the corresponding AATS values. This happened because the MODIS aerosol cloud mask selectively removed 0.5 km pixels containing smoke and clouds before the aerosol retrieval. The other two coincidences (one Terra and one Aqua) occurred during one P-3 flight on the same day and in the same general area, in an atmosphere characterized by a relatively low AOD (< 0.3), and spatially homogeneous regional haze from smoke outflow with no distinguishable plume. For the ensemble data set for MODIS AOD retrievals with the highest-quality flag, MODIS AOD agrees with AATS AOD within the expected MODIS over-land AOD uncertainty in 60 % of the retrieval grid cells at 10 km resolution and 69 % at 3 km resolution. These values improve to 65 % and 74 %, respectively, when the cloud-contaminated case with the strongest plume is excluded. We find that the standard MODIS dark-target over-land retrieval algorithm fails to retrieve AOD for thick smoke, not only in

ACPD
13, 15007–15059, 2013

cloud-contaminated regions, but also in clear sky. We attribute this to deselection, by the cloud and/or bright surface masks, of 0.5 km resolution pixels that contain smoke.

1 Introduction

The 14-channel Ames Airborne Tracking Sunphotometer (AATS-14 or AATS) was operated on a NASA P-3 aircraft based in Cold Lake, Alberta, Canada during the summer phase of the 2008 Arctic Research of the Composition of the Troposphere from Aircraft and Satellites (ARCTAS) field campaign (Jacob et al., 2010). AATS measurements were analyzed to calculate aerosol optical depth (AOD) at 13 wavelengths (354–2139 nm), and columnar water vapor (CWV) in nine flights that sampled smoke from boreal forest fires, Asian outflow, and emissions from mining sites. In this paper, we use only a limited subset of the ARCTAS summer AATS AOD data set. We compare AATS AOD from five short time segments of four P-3 flights with AOD retrieved by the Moderate Resolution Imaging Spectroradiometer (MODIS) dark-target land aerosol retrieval algorithm from measurements acquired over land during one Terra and four Aqua satellite overpasses that were spatially and temporally near-coincident with the AATS measurements.

Our paper is the fourth in a series of studies that use AATS data obtained during ARCTAS. Shinozuka et al. (2011) provided a detailed overview of AOD calculated from AATS measurements during the spring and summer phases of ARCTAS. They focused on data obtained during aircraft vertical profiles, for which they compared AOD magnitude and spectral behavior, in addition to particle fine-mode fraction calculated from AATS data, with parameters derived from P-3 in situ sensor measurements. They also examined the consistency between AATS and ground-based full-column AOD using measurements obtained during flyovers of five sites of the Aerosol Robotic Network (AERONET) (Holben et al., 1998). Shinozuka and Redemann (2011) used AATS AOD to conduct a statistical study on the horizontal variability of AOD during both phases of

ACPD
13, 15007–15059, 2013

ARCTAS. Segal-Rosenheimer et al. (2013) used AATS measurements in ARCTAS to demonstrate a new approach to retrieving cirrus properties.

Our investigation compares AATS AOD with MODIS Collection 6 (C006) AOD retrievals at 10 km × 10 km and 3 km × 3 km (at nadir) spatial resolution over land. Most studies (Chu et al., 2002; Remer et al., 2005, 2013; Levy et al., 2005, 2007a,b, 2010) that have addressed validation of MODIS aerosol retrievals over land have relied solely on ground-based sunphotometer measurements from AERONET, and have benefitted from the large number of available MODIS/AERONET coincident measurements. Studies to validate MODIS over water aerosol retrievals have used either data from AERONET coastal or island sites (e.g., Levy et al., 2005; Redemann et al., 2005) from shipboard measurements by handheld devices as part of the Maritime Aerosol Network (Kleidman et al., 2012), or have used over-water airborne sunphotometer measurements from AATS-6 or AATS-14 (Schmid et al., 2003a,b; Livingston et al., 2003, 2009; Redemann et al., 2005, 2006; Russell et al., 2007), for which the number of coincident data sets is limited. All of the studies referenced above dealt with validation of the 10 km resolution aerosol product retrieved by the MODIS over-water or over-land operational algorithms. Other retrieval algorithms have been developed and applied to MODIS data to yield aerosol retrievals at finer resolution for local areas of interest (C. Li et al., 2005; Castanho et al., 2008), or for global application (Lyapustin et al., 2011). Remer et al. (2013) provide a detailed description of the C006 MODIS 3 km aerosol retrieval algorithm, and compare six months of Aqua AOD (retrieved from measurements collected over three separate years) with values calculated from collocated AERONET measurements. Munchak et al. (2013) further investigate the usefulness and validity of the MODIS 3 km product over an urban/suburban landscape by comparing the product with a mesoscale array of 40 AERONET stations and an airborne High Spectral Resolution Lidar.

The five MODIS/AATS near-coincident measurement events analyzed in this paper represent the largest number of over-land intercomparisons from a single AATS field mission. More importantly, they represent the first comparison of airborne

ACPD
13, 15007–15059, 2013

sunphotometer AOD with the MODIS C006 10 km and the new 3 km resolution over land aerosol retrieval products. Consistent with the approach in previous AATS/MODIS comparisons, we take advantage of the high temporal (one 3 Hz 3 s average every 4 s) and spatial (~ 360 m/3 s average in the horizontal) resolution, and the areal extent of the AATS measurements, to compare AATS and MODIS AOD within individual MODIS aerosol retrieval grid cells that intersected the P-3/AATS track. There were a total of 58 10 km and 134 3 km grid cells that have AOD available from both (1) the standard MODIS operational algorithm retrievals and (2) calculations from AATS measurements.

The high-spatial-resolution AATS measurements obtained during ARCTAS present a unique opportunity to examine the impact of spatial variability on over-land MODIS AOD retrievals. Yet, we recognize there are limitations to the analyses. First, the number of available intercomparisons is limited to five MODIS overflights, and as we shall show, clouds further limited the availability of MODIS retrieval cells and confounded the comparisons in two of these cases. Secondly, there are inherent differences between the MODIS and AATS sensors that make such comparisons problematic. MODIS is a downward-viewing satellite sensor that measures upwelling Earth-atmosphere reflectance, and AATS is a Sun-viewing airborne sensor that measures transmission of the direct solar beam through the atmosphere above the aircraft. Invariably, there are temporal and spatial sampling differences. MODIS measurements within a satellite aerosol retrieval grid cell are essentially instantaneous compared to the AATS measurements. During ARCTAS, the latter were acquired over the time period, ranging from several seconds to a few minutes, that it took the P-3 to traverse some small fraction of each satellite retrieval grid cell. Because the respective sensor viewing geometries are significantly different, so too are the respective air parcel volumes sampled. Hence, spatial inhomogeneity of the aerosol, especially within a smoke plume, can lead to significant differences in the retrieved AODs. This is further complicated by the limited coverage and by the location of the specific track of the aircraft within each MODIS retrieval grid cell.

ACPD
13, 15007–15059, 2013

2 Sensors and aerosol retrieval algorithms

2.1 MODIS

The MODIS instruments aboard the Terra and Aqua satellites measure radiance in 36 visible, near-infrared, and infrared spectral bands between 415 and 14 235 nm (King et al., 1992), using different spatial resolutions of 0.25, 0.50, or 1 km, depending on the particular band. MODIS views a swath ∼ 2300 km wide that is broken into 5 min "granules", each ∼ 2030 km long. The MODIS over-ocean operational algorithm for the retrieval of AOD has been described in detail by Remer et al. (2005). The MODIS dark-target over-land retrieval algorithm is based on work by Kaufman et al. (1997). As noted by Levy et al. (2010), the second-generation over-land dark-target algorithm was developed by Levy et al. (2007a,b; 2009) and addressed issues identified in previous versions of the MODIS dark land aerosol product (e.g., Remer et al., 2005; Levy et al., 2005). Levy et al. (2013) describe in detail the MODIS Collection 6 aerosol products and the differences between the Collection 5 and Collection 6 algorithms. Remer et al. (2013) discuss the new 3 km resolution C006 aerosol products, and present an initial comparison of the MODIS AOD retrievals and collocated AERONET AODs on a global basis. Munchak et al. (2013) focus on the mid-Atlantic region of the US and make use of a mesoscale grid of approximately 40 AERONET instruments to evaluate the 3 km resolution product across an urban/suburban landscape.

The MODIS retrieval algorithm over land (both 10 km and 3 km) performs a simultaneous inversion of the measured top of the atmosphere reflectance in three channels (centered at wavelengths, λ, of 466, 645, and 2113 nm) to retrieve total spectral AOD, "fine" model weighting parameter, and surface reflectance at 2113 nm. This is done by comparing measurements to pre-computed lookup tables (LUT) of simulated TOA reflectance for five aerosol types (Levy et al., 2007a), loadings, and observing geometry, but with a number of constraints. These constraints include: (a) assigning a fine-dominated aerosol type (fine-model) for a given location and season; (b) requiring the fine-model to be mixed with a coarse-dominated (dust) model, with some

ACPD
13, 15007–15059, 2013

to-be-determined weighting (ETA); and (c) the surface optical properties must be spectrally related. Specifically, for our ARCTAS region, the moderately absorbing fine-model is assumed. The principal product is AOD at 553 nm, but since the LUT is indexed, the AOD can also be determined at the other three wavelengths (466, 645, and 2113 nm). From this information, one can also calculate such properties as fine-model AOD (fAOD = ETA · AOD) and extinction Ångström exponent (AE). Although these derived parameters (fAOD and AE) were included in C005 products, Levy et al. (2010) concluded that these size parameters in the over-land data set have little physical validity, and instead primarily reflect algorithm assumptions about particle type. Hence, only the directly retrieved fine-model weighting parameter has been retained as a product in the C006 aerosol data set. Although the AE is not retained as a product, we can easily calculate AE offline (the negative slope of a linear least-squares fit of log(AOD) vs. log(λ) using only AOD from the three shortest MODIS AOD wavelengths).

The retrieval technique is the same for creating the 3 km and 10 km data products. Although the MODIS C006 aerosol products are provided at these (nadir) resolutions, the algorithm uses the higher-resolution MODIS observations (e.g., 0.5 km × 0.5 km or 1 km × 1 km data). This is done to increase signal to noise, and to have the flexibility to filter out or "mask" pixels that are not appropriate for clear-sky, dark-target aerosol retrieval, including clouds, snow/ice, inland water, and bright reflecting surfaces. As described (e.g. Levy et al., 2010; Remer et al., 2012), several tests are applied (Martins et al., 2002; Ackerman et al., 1998; R. Li et al., 2005) to remove these inappropriate pixels. The first "test" is actually a set of multiple tests to mask cloudy pixels. The cloud mask is primarily based on spatial variability of reflectance, and results in a designation of "cloudy" or "cloud free" for each 0.5 km resolution pixel. In the MODIS C006 product, this resulting cloud mask is reported as Aerosol_Cldmask_Land_Ocean. In the first sub-test (Martins et al., 2002), the standard deviation is calculated for each set of 3 × 3 0.5 km resolution reflectances (applied to the 466 nm channel for over-land retrievals); if the standard deviation exceeds a designated value, then the center pixel of the 9 pixels is designated "cloudy". Spatial variability is also calculated using the 1382 nm

ACPD
13, 15007–15059, 2013

channel at 1 km resolution. This channel is sensitive to the upper atmosphere, and to cirrus clouds in the upper atmosphere. Smooth, thin cirrus that might escape identification as clouds in the 466 nm spatial variability can sometimes be identified with this cirrus-sensitive channel. Over land, pixels that include inland water, snow (R. Li et al., 2005), and bright land surfaces are then deselected based on information provided as input, pixel brightness, and several internal algorithm tests. For example, pixels with calculated values of the Normalized Difference Vegetation Index (NDVI) less than 0.1 are believed to be "inland water bodies" and are masked.

At the end of the masking procedures, all the pixels that have escaped masking and are considered ready for retrieval are ordered according to their reflectance at 645 nm. The darkest 20 % and the brightest 50 % of these remaining and "good" pixels are arbitrarily discarded, and the procedure continues with only 30 % of the unmasked pixels. The land algorithm requires a minimum of 12 remaining pixels (10 % of a possible 120) to attempt a retrieval at 10 km, and at least 50 pixels (42 %) to receive consideration as a very-good quality retrieval. To attempt a 3 km retrieval, the algorithm requires at least 5 pixels (45 % of a possible 11). The number of pixels used in each 3 km or 10 km retrieval is reported in the MODIS C006 product as Number_Pixels_Used_Land.

Most diagnostics available at 10 km are also included in the archived data files for the 3 km product (Remer et al., 2013). These include a Quality Flag (QF) that classifies each retrieval as bad (0), marginal (1), good (2), or very good (3); the number of 0.5 km × 0.5 km pixels used in the retrieval, and the assigned fine-model aerosol type.

2.2 AATS-14

The AATS-14 instrument measures the atmospheric transmission of the direct solar beam in 14 spectral channels with center wavelengths ranging from 354 to 2139 nm, and full width at half maximum (FWHM) bandwidths of ∼ 5 nm (exceptions are 2.0 nm for the 354 nm channel and 17.3 nm for the 2139 nm channel). The instrument has been described in detail in several previous publications (e.g., Russell et al., 2005, 2007; and references therein). Our methods for data acquisition and analysis have been well

ACPD
13, 15007–15059, 2013

documented in the literature (Russell et al., 1993a,b; Schmid and Wehrli, 1995; Schmid et al., 1996, 1998, 2001, 2003; Livingston et al., 2005, 2007). Most recently, citing the previous publications, Shinozuka et al. (2011) detailed these procedures. We provide only a brief synopsis here.

The AATS channel wavelengths were chosen to permit separation of aerosol, water vapor, and ozone transmission along the AATS-to-Sun slant path. During ARCTAS, data were sampled at 3 Hz and recorded as 3 s averages together with the sample standard deviations over the nine samples. We routinely calculate spectral AOD from detector voltages measured in 13 of the 14 AATS channels. Calculation of AOD(λ) requires knowledge of exoatmospheric detector voltages, $V_0(\lambda)$. For the data we present here, the $V_0(\lambda)$ values were based on sunrise measurements acquired at Mauna Loa Observatory, Hawaii, in May 2008. In accord with the procedure described in Schmid et al. (2003a,b), these values were then adjusted by analysis of high-altitude clear air AOD spectra obtained during the deployment. AATS measurements were screened to remove data points that include clouds by using both the standard deviations of the raw voltages and the shape of the spectral AOD signature.

3 Results

3.1 Overview of ARCTAS data cases and analysis approach

We compare AATS and MODIS AOD retrieved from measurements acquired over land during four P-3 flights that included five satellite overpasses on 30 June (Aqua), 2 July (Aqua), 3 July (Terra and Aqua), and 9 July (Aqua) 2008. On 30 June, the P-3 intersected a well-defined smoke plume in a clear-to-mostly-clear sky at the exact time of the Aqua overpass. The 2 July case was marked by smoke beneath scattered cirrus and cumulus clouds and a rather complicated P-3 horizontal flight track. The two 3 July coincidences were characterized by a relatively small AOD (< 0.3), spatially homogeneous regional haze from smoke outflow with no distinguishable plume (Shinozuka

ACPD
13, 15007–15059, 2013

et al., 2011) in mostly clear sky. The locations of the coincident MODIS aerosol grid cells and the P-3 track were within 25 km for the morning Terra and afternoon Aqua overpasses, which occurred about 3 h apart. The 9 July case involved a general south-north P-3 flight track characterized by smoke beneath scattered clouds.

In each case, we limit the comparison to AATS data collected at minimum P-3 altitude (~ 100–600 m a.g.l.) within intersecting MODIS aerosol retrieval grid cells during short-duration, primarily horizontal flight segments within a few minutes of the time of the satellite overpass. The duration of the flight segments was 12–17 min for the 30 June, 3 July, and 9 July cases, and 48 min for the 2 July case; temporal differences between the AATS measurements and the MODIS overpass were 0–20 min for 30 June, 3 July, and 9 July, and 7–55 min for 2 July. For each MODIS overpass, we first calculate the mean AOD spectrum from all cloud-screened AATS measurements within each MODIS grid cell. Then, we interpolate using a second-order polynomial in log(AOD)–log(λ) space for the 11 AATS channels centered at wavelengths between 353.5 and 1019.1 nm to calculate AATS AOD at the MODIS wavelength of 553 nm. To compare MODIS full-column AOD retrievals with AATS above-aircraft AOD, it is necessary to increase each AATS AOD by the amount of AOD between the surface and the altitude of the P-3. We have estimated this amount by assuming a constant below-aircraft aerosol extinction spectrum profile equal to the extinction coefficient calculated from simultaneous measurements at flight level by the P-3-based University of Hawaii HiGear in situ suite of instruments, as described in Shinozuka et al. (2011). These instruments included two three-channel (450, 550, 700 nm) TSI model 3563 integrating nephelometers (Anderson et al., 1996, 2003; Heintzenberg and Charlson, 1996), and two three-wavelength (470, 530, 660 nm) Radiance Research particle soot absorption photometers (PSAPs). After interpolation to 553 nm, the below-aircraft AOD estimates were added to the mean AATS AODs within each grid cell to yield adjusted AODs. However, we note that the uncertainty in the estimated below-aircraft AOD can be particularly large within a smoke plume due to the assumption of vertical homogeneity in aerosol extinction below the aircraft, and that there is no way to validate these estimates

ACPD
13, 15007–15059, 2013

for the cases discussed here. Hence, we have chosen to use both the unadjusted and adjusted AATS AODs in our analyses, but have been careful to repeatedly inform the reader exactly what we are showing to avoid confusion. For comparison of MODIS and AATS AE, we calculate AATS AE values using only AATS AOD calculated from measurements in the five channels centered at wavelengths between 451 and 675 nm. In particular, the AATS AE are calculated as the negative slope of a linear least-squares fit of log(AOD) vs. log(λ) for AATS channels centered at λ = 451, 499, 520, 606, and 675 nm.

For each case, we show the MODIS RGB image with locations of the P-3/AATS flight track and the MODIS 10 km aerosol retrieval grid cells overlaid. We also present a map view that overplots the P-3 flight track color-coded by AATS AOD at 520 nm on color-coded boundaries of the MODIS 10 km retrieval grid cells intersecting the P-3 track, and (in a separate figure) the MODIS 3 km retrieval grid cells that either intersect (green) the P-3 track or intersect (black) a MODIS 10 km grid cell. We also show a color-coded multiframe graph that overplots the corresponding retrieved MODIS and the calculated AATS AOD spectra (the latter before any wavelength interpolation or adjustment due to estimated AOD below the P-3) within the 10 km MODIS grid cells. Graphs of AOD (at 553 nm) as a function of latitude or longitude are used to overlay unadjusted and adjusted AATS AOD with MODIS 10 km and 3 km AOD along the flight track. Scatterplots compare mean MODIS 3 km AOD within the MODIS 10 km grid cells, and compare the MODIS 10 km and 3 km AODs with the corresponding mean of the AATS AODs at 553 nm. Following the analyses of the individual cases, we examine composite scatterplots that compare MODIS and AATS AODs, and MODIS and AATS AE, for all grid cells. Table 1 lists MODIS and AATS AOD at 553 nm, AE, and other parameters pertaining to the comparisons within the 10 km retrieval grid cells. Corresponding scatterplot statistics are summarized in Table 2 (AOD) and Table 3 (AE).

ACPD
13, 15007–15059, 2013

3.2 30 June 2008

On 30 June, we acquired AATS-14 measurements during a NW–SE aircraft transect at an altitude of 102–218 m a.g.l. during the time period 19.67–19.95 UT, bracketing the time of the Aqua-MODIS satellite overpass at 19.84 UT. The measurements were focused on a thick smoke plume originating from a forest fire located at ∼ 58.43° N, 106.76° W in north-central Saskatchewan. AATS measurements yielded mid-visible (520 nm) AODs that ranged from 0.05 in clear air outside the smoke plume, to > 2 in the plume, with corresponding AE of 1.56 to 2.16, respectively.

Figure 1a shows the Aqua MODIS RGB image at the time of satellite overpass, the locations of the 13 MODIS C006 operational 10 km aerosol retrieval grid cells, and the location of the P-3/AATS flight track during the 19.67–19.95 UT period. The smoke plume dominates the scene, and it is apparent that the projected P-3 track intersected the plume at the exact time of the MODIS overpass. In fact, the P-3, flying at an altitude of ∼ 125 m a.g.l., actually penetrated the plume. Scattered to broken clouds are evident in the area well north of the plume, but the southern two-thirds of the scene, including the region of the smoke plume and most of the P-3 flight track, appears to be cloud-free, although this image alone cannot be used to completely rule out very small scattered cumulus or thin cirrus. In Fig. 1b, the P-3 flight track is plotted as color-coded AATS-derived AOD at 520.4 nm, and the locations of the 10 km resolution grid cells (color-coded by location for subsequent comparison with AATS AOD spectra) that intersect the P-3 flight track are also shown. These are overlaid on a contour plot of MODIS 553 nm AOD retrieved with both the aerosol cloud mask and the NDVI mask turned off (see discussion in the next paragraph). The contours are shown only for illustrative purposes to identify the location of the smoke plume relative to the P-3 flight track. In Fig. 1c, AATS AODs at wavelengths 451.2, 520.4, and 675.1 nm, and the corresponding AATS AE, are plotted as a function of time and latitude. The solid magenta squares show AE calculated from the mean of the AATS AODs located within each MODIS aerosol retrieval grid cell and plotted at the mean time of the AATS measurements

ACPD
13, 15007–15059, 2013

within each grid cell. Values of AE outside the plume were 1.5–1.8, which indicates that the AATS cloud filter was effective in removing any optically thick cloud-contaminated observations, for which an AE near zero would be expected. Values of AE inside the plume were 2.1–2.2, indicative of the fresh smoke small particles.

Figure 2 displays the results of MODIS AOD retrievals at 10 km and 3 km resolution for three scenarios: (1) the standard operational retrieval (a, d), (2) aerosol cloud mask off (b, e), and (3) aerosol cloud mask and NDVI mask off (c, f). In each frame, the MODIS 553 nm AOD has been color-coded by magnitude and overlaid on the same RGB image shown in Fig. 1a; the P-3 flight track is shown for reference. Regions with no color-coded AOD are those for which there was no MODIS AOD retrieval, and it is clear that the standard operational retrieval algorithm masks a significant number of grid cells in the heart of the smoke plume at both 10 km (Fig. 2a) and 3 km (Fig. 2d) resolution. Comparison of the corresponding frames (b, e and c, f) for retrieval scenarios 2 and 3 reveals that application of both the aerosol cloud mask and the NDVI mask limited the number of retrievals within the smoke plume, especially west of the P-3/AATS track. Fortunately, however, our focus in this paper is on those grid cells that intersect the P-3 flight track, and we note that the MODIS operational retrieval algorithm actually retrieved AOD in all 10 km grid cells located along that segment of the P-3 flight track inside the smoke plume. However, it failed to retrieve AOD in two 3 km grid cells in the heart of the plume along the flight track. There were also two 3 km grid cells with no AOD retrieval along the flight track south of the plume. However, the AATS cloud filter also identified the region just south of the plume as cloud-contaminated, and this is reflected in missing AOD data points at $\sim 58.03^{\circ}$ N in Fig. 1c.

Figure 3 presents detailed results of the AATS/MODIS comparisons, and Table 1 lists detailed results for the AOD retrievals in each 10 km grid cell along the P-3 flight track. Frames 3a, c, d, and e show results for the MODIS standard (cloud mask and NDVI mask on) AOD retrievals only, while frame b includes MODIS AOD spectra retrieved with and without the cloud and NDVI masks. Figure 3a shows the locations of the AOD color-coded MODIS 10 km retrieval grid cells (red) and the 3 km cells (green) that

ACPD
13, 15007–15059, 2013

intersect the P-3 track, in addition to all 3 km cells (black) that intersect a 10 km cell but not the P-3 track.

Figure 3b overplots corresponding calculated AATS and retrieved MODIS AOD spectra in cells 2–13 of the 13 intersecting MODIS 10 km grid cells. Cell 1, the northernmost cell, has been omitted to maximize the size of the display. AODs are shown only for the three shortest MODIS wavelengths and for the seven AATS channels between 354 and 675 nm. As noted in Sect. 3.1 above, in this and subsequent spectral AOD plots, we purposely show the calculated AATS AODs without any adjustment for the estimated AOD below the P-3 altitude. However, Table 1 lists AATS AOD at 553 nm and AE before and after addition of the estimated below-aircraft AOD. MODIS spectra are shown for the standard retrievals and with the cloud and NDVI masks off, and the spectra are color-coded using the same color scheme as that used in Fig. 1b. Plots are arranged and labeled numerically from north to south along the P-3 flight track. The AATS data points represent the mean of all cloud-free AATS retrievals within each corresponding MODIS grid cell; the vertical bars give the sample standard deviation (wide horizontal ticks) and range (narrow ticks) within the cell. Typically, AATS measurement uncertainties for an individual observation were much less than either the sample standard deviation or the range of AATS-derived AOD for a particular MODIS grid cell. The vertical bars plotted on the standard MODIS retrievals represent the expected error (EE), $\pm$ (0.05 + 0.15AOD), for the over-land AOD retrieval (Remer et al., 2005; Levy et al., 2010). All standard MODIS AOD retrievals yield a QF of 3 (Table 2), and used a moderately absorbing fine-mode aerosol (type 2, not listed in Table 2).

Figure 3b shows that MODIS AODs agree with AATS values (calculated before the addition of estimated AOD below the aircraft) to within the MODIS EE in most 10 km grid cells. Table 2 indicates that MODIS retrievals agree with the adjusted AATS AODs to within EE in 10 of 13 10 km grid cells. Table 1 reveals that the two 10 km grid cells (numbers 7 and 8 in the heart of the plume in Fig. 1b) with the largest MODIS and AATS AODs are among the ten cells in agreement. The MODIS aerosol cloud mask deselected 49 and 16 0.5 km pixels, respectively, and the NDVI mask deselected an

ACPD
13, 15007–15059, 2013

additional 15 and 3 0.5 km pixels, respectively, in these two grid cells. Table 1 indicates further that there is no significant difference between the MODIS retrievals performed with and without the cloud and NDVI masks. The difference between MODIS AODs and adjusted AATS AODs falls outside the MODIS EE only in cells 4, 9, and 10; these are discussed below.

First, we focus on the individual data points while momentarily ignoring the MODIS uncertainty bars. The MODIS AOD spectrum in cell 2 (58.69° N, north of the smoke plume) significantly underestimates the mean AATS spectrum, and we have no explanation. The MODIS RGB image (Fig. 1) indicates that there were some clouds in cells 1 and 2, but the AATS data in both cells have been cloud-screened, and since resultant AOD spectra along the flight track through the two cells are essentially equal (c.f., Fig. 3b, c and Table 1), there is no indication that the AATS spectra are cloud-contaminated. The MODIS spectrum in cell 4 (58.51° N, north of the smoke plume) overestimates the AATS values; there are at least two plausible explanations for the overestimate. The MODIS retrieval may still include residual cloud-contaminated reflectances, perhaps evidenced by the low MODIS AE of 0.62 versus 1.72 for the AATS spectrum. However, we note again the Levy et al. (2010) finding that the MODIS AE does not contain reliable particle size information. Secondly, the RGB image in Fig. 1 indicates that MODIS may have actually measured aerosol in the western portion of grid cell 4, whereas AATS would not have seen this aerosol, because the P-3 track traversed only the far eastern portion of the MODIS grid cell. Although the agreement between MODIS and AATS AOD data points seems particularly good in cells 5–8 (including cells 7 and 8 in the center of the plume), the MODIS spectrum in cell 8 is much flatter (AE = 0.62) than the corresponding AATS spectrum (AE = 2.15). As shown in Table 1, MODIS AODs significantly underestimate the AATS values (by ∼ 60 %) in the two southernmost cells (9-dark green, and 10-light green) that intersect the smoke plume, but this can probably be explained by a combination of horizontal inhomogeneity within the plume and different instrument sampling regions. In particular, cell 9 includes a large region of less optically dense smoke, whereas AATS viewed through the heart

ACPD
13, 15007–15059, 2013

of the plume along the P-3 track in the far eastern portion of the MODIS cell. A large portion of cell 10 was outside the smoke plume, but similar to the AATS measurements along the P-3 track through cell 9, AATS viewed the sun through much greater smoke concentrations located only in the northeastern portion of cell 10. This was also the region where some AATS data points were excluded by the AATS cloud filter. As can be seen in Fig. 3c and e (less obvious), the MODIS retrieval plus EE in cell 10 barely falls below the AATS mean value.

Figure 3c displays the latitudinal variation of AOD by overplotting MODIS AODs retrieved at 553 nm for both spatial resolutions and AATS AODs (with and without the addition of estimated AOD below the aircraft) interpolated to 553 nm. Also plotted are values of the mean and standard deviation of the MODIS retrievals in all 3 km grid cells intersecting each 10 km cell. MODIS retrievals at both resolutions successfully track the plume, but the 3 km AODs are noisier than the 10 km values. A scatterplot of MODIS 3 km vs. MODIS 10 km AOD (553 nm) is presented in Fig. 3d, where the mean (symbol) and sample standard deviation (vertical bar) AODs have been calculated from all MODIS 3 km retrieval grid cells intersecting each 10 km grid cell. The comparison yields a high coefficient of determination (R^2) of 0.986, with a mean difference and root mean square difference (RMSD) of 6.8 % and 26 %, respectively (rightmost columns of Table 2). Figure 3e presents corresponding scatterplots of MODIS 3 km and 10 km retrievals versus the mean of the adjusted AATS AODs (labeled AOD AATS adj HG) calculated within the 3 km and 10 km MODIS grid cells. The dashed line shows the 1 : 1 correspondence, and the dashed curves display the one standard deviation expected MODIS over-land AOD retrieval uncertainties. The MODIS EE curves (Remer et al., 2005; Levy et al., 2010) for the 10 km retrievals are defined above in this section; the EE curves for the 3 km retrievals equal ± (0.05 + 0.25 AOD) (Remer et al., 2013). Table 2 lists values of R^2, mean difference, and RMSD pertaining to each pair of data sets shown in this and subsequent scatterplots. The statistical parameters are not remarkably different for the MODIS 10 km and 3 km retrievals with the cloud and NDVI masks on and off (not shown). In comparing the AATS and MODIS retrievals, the

ACPD
13, 15007–15059, 2013

3 km MODIS retrievals (with masks on or off) are noisier than the corresponding 10 km retrievals, with the former yielding lower values of R^2, and higher mean difference and RMSD values.

3.3 2 July 2008

In this section, we compare AATS AODs derived from measurements acquired on 2 July during the time period 19.7–20.5 UT with AODs retrieved from collocated MODIS measurements taken during an Aqua overpass at 19.58 UT. During this time, the P-3 performed various cross-plume and along-plume maneuvers at altitudes 210–420 m a.g.l. to sample smoke originating from two separate fires. This case is particularly challenging for comparing AATS and MODIS AOD retrievals due to scattered clouds above the smoke. This is evident in Fig. 4, which overlays on the MODIS RGB image the locations of the P-3 flight track and the MODIS 10 km retrieval grid cells for the operational retrieval, and for retrievals with either the aerosol cloud mask off or with the aerosol cloud and NDVI masks off (see below and Fig. 4 caption for details).

Figure 5a overlays the locations of the MODIS 10 km grid cells and the color-coded, cloud-screened AATS 520 nm AOD along the P-3 flight track. The MODIS grid cells have been numbered in chronological order along the P-3 flight track for comparison of MODIS and AATS AOD spectra in Fig. 5b. For those few MODIS grid cells that included multiple P-3 flight intersections at different times and in different directions, we have used the time of the first intersection to order each cell. Red cell boundaries with black cell numbers identify those cells (18 total) for which the MODIS standard operational algorithm produced an AOD retrieval; magenta cell boundaries and numbers identify cells for which the algorithm produced a retrieval only with the aerosol cloud mask (or with the cloud mask and the NDVI mask) off. Figure 5b overplots MODIS and unadjusted AATS AOD spectra for 30 of the 32 grid cells shown in Fig. 5a (cells 9 and 11, for which there was no MODIS AOD retrieval with the masks on, have been omitted to facilitate display of the multi-frame plot). MODIS spectra are displayed for retrievals with cloud mask off, with cloud and NDVI masks off, and (for the 18 cells referenced

ACPD
13, 15007–15059, 2013

above), for the operational retrievals (i.e., with both masks on). Each frame is annotated with the cell number and the MODIS retrieval QF for the standard (i.e., masks on) retrieval. Quality flag values are not meaningful, and hence are not shown for the retrievals with the masks off. Based on the MODIS RGB image in Fig. 4 and the magnitude of the AATS AOD spectra in Fig. 5b, we conclude that smoke dominated the AATS measurements in 12 of the 30 cells displayed in Fig. 5b: cells 30–32 in the far north; 10 and 12 (and also cells 9 and 11 not shown) in the west; and 1, 2, 6, and 17–20 in the center. We note that all MODIS retrievals used a moderate absorption fine-mode aerosol type.

We include MODIS AOD retrieved with the aerosol cloud mask off and with the cloud and the NDVI masks off in Fig. 5b and Table 1 to suggest that although the standard MODIS retrieval algorithm failed to retrieve AOD in the heart of the plumes due to clouds, there might be information in the MODIS reflectances. We call the reader's attention to the MODIS "cloud-contaminated" AOD spectra in Fig. 5b in the heart of the eastern plume in cells 1, 2, 17, 18, and 19, and even in cells 8 and 10 of the western plume. It is beyond the scope of this paper to pursue extracting aerosol information from these "cloud-contaminated" MODIS retrievals. Furthermore, although we show these MODIS retrievals, and at least in that sense, do compare them with the AATS values, we do not include them in AOD scatterplots in subsequent figures or in the statistics listed in Tables 2 and 3. This is because the 2 July coincidence region was obviously greatly affected by clouds in addition to smoke, unlike the 30 June region, for which a well-defined smoke plume was located in clear to mostly clear sky.

Figure 6 takes a more detailed look at the AATS/MODIS AODs presented in Fig. 5b by displaying various parameters as a function of cell number for all 32 cells highlighted in Figs. 4 and 5a. In Fig. 6, we include results for the MODIS operational retrieval and for the retrieval with the aerosol cloud mask off, but we do not show any results for the retrieval with both the aerosol cloud and the NDVI masks off. Figure 6a shows mean AATS interpolated 553 nm AODs, both with and without addition of the in situ estimate of the below-aircraft AOD, and the corresponding MODIS minus AATS AOD

ACPD
13, 15007–15059, 2013

differences with and without below-aircraft AOD. We note that the below-aircraft AOD estimates are very large (up to 1) in the heart of the eastern plume in cells 1, 2, 16–20; and significant in cell 6 of the eastern plume and in cells 10–12 of the western plume. We cannot validate these estimates, but we recognize that the very large values may be suspect, especially for cases when the smoke plumes do not extend vertically to the ground as our extrapolation method assumes. Figure 6b shows the AATS AOD AE (calculated without the addition of estimated below-aircraft AOD) and corresponding MODIS minus AATS AE differences. The standard MODIS AOD retrieval QF values are plotted in Fig. 6c. Figure 6d displays the number of pixels used in the MODIS retrieval for each cell, and also the number of AATS AOD measurements within each cell.

Figure 6a, b indicate that AATS mean AODs and AE are somewhat positively correlated (R^2 = 0.52). Because the AATS data processing cloud filter, which relies both on raw signal variation during the 3 s sampling period and on spectral AOD shape, may not remove all cloud-contaminated measurements for spatially homogeneous clouds, such as thin cirrus with small OD compared to the total AOD (Redemann et al., 2005), we cannot say with absolute certainty that all cloud-affected data points have been removed from the 2 July measurements. However, the relative contribution of residual cloud to the total AOD is likely quite small, as AATS Ångström exponents exceeded 0.95 in all 32 cells, and the cells (1, 2, 10–12, 17–20, 30–32) with the largest mean AOD values had AE > 1.7. The MODIS AE values show no correlation with the AATS values (see also Table 3), but this is not surprising in light of the above-mentioned finding by Levy et al. (2010). Hence, we focus on comparison of MODIS and AATS AOD.

Figure 7 examines the operational MODIS AOD retrievals as a function of the MODIS retrieval QF: (a) QF ≥ 0, (b) QF ≥ 1, (c) QF ≥ 2, and (d) QF = 3. Frames on the left overlay the AATS-AOD color-coded P-3 flight track on the locations of the MODIS 10 km and 3 km retrieval grid cells, analogous to Fig. 3a. The right frames display scatterplots of MODIS and AATS AODs and are analogous to Fig. 3d and e. Although only a few 3 km

ACPD
13, 15007–15059, 2013

retrievals intersect each 10 km grid cell, the MODIS results at these two resolutions are mutually consistent, as shown in the left scatterplots and in Table 2. Of 18 10 km retrievals, only 12 had QF ≥ 2 and only 6 had the highest QF = 3. If we compare the MODIS and AATS AODs (AATS values adjusted for the below-aircraft AOD), only 43 % of the MODIS 10 km retrievals with values of QF ≥ 1 and 33 % (two of six) of those with QF = 3 fall within the MODIS EE. Most of the MODIS retrievals with QF ≥ 1 underestimate AATS AOD by greater than the EE (see Table 2, column labeled "< AATS AOD"). None overestimates AATS AOD. Values of R^2 increase with increasing QF, but R^2 is still only 0.37 for the six QF = 3 retrievals. MODIS AOD retrievals significantly underestimate the AATS values (by 60–80 %), but values of the mean difference and RMSD are not markedly different for different ranges of QF included. Of only 25 retrievals at 3 km resolution, 23 had QF = 3 and the other two had QF = 0. Of those with QF = 3, 43 % fall within MODIS EE when compared with the AATS values, but 52 % underestimate AATS AOD by greater than the EE. Mean MODIS-AATS differences were ∼ 40 %, with RMSD values of ∼ 77 %, both of which are smaller than for the 10 km retrievals.

3.4 3 July 2008

On 3 July there were separate AATS/MODIS Terra and AATS/MODIS Aqua coincidences near 55.7° N, 112.2° W in east central Alberta. As shown in Fig. 8, the MODIS Terra overpass occurred at 18.50 UT, and coincident AATS measurements were taken during a NW–SE horizontal transect at a mean ± one standard deviation altitude of 0.176 ± 0.054 km a.g.l. during the time period 18.45–18.7 UT. The MODIS Aqua overpass occurred at 20.33 UT, and AATS measurements were acquired during the period 20.40–20.66 UT along a P-3 flight track that included a short longitudinal transect followed by a series of constant altitude circles, with a mean altitude for the entire flight segment of 0.203 ± 0.041 km a.g.l. The weather was clear for both flight segments, and the aerosol overburden was small, with AATS mid-visible AODs 0.21–0.26 for the Terra overpass and 0.22–0.24 for the Aqua overpass. Shinozuka et al. (2011) characterized the aerosol as an outflow of smoke with no distinguishable plume. Figure 8 displays

ACPD
13, 15007–15059, 2013

the MODIS RGB image, the P-3 flight track, and the MODIS 10 km AOD retrieval grid cells for the two MODIS overpasses.

AATS measurements are compared with MODIS operational AOD retrievals within 12 MODIS 10 km resolution AOD retrieval grid cells and 44 3 km grid cells for the Terra overpass. Figure 9 presents the results. Figure 9a overlays the P-3 flight track color-coded by the AATS 520 nm AOD and the locations of the MODIS 10 km and 3 km resolution grid cells. Corresponding MODIS and AATS AOD spectra within each 10 km grid cell are overplotted in Fig. 9b. Analogous to the spectra shown in Figs. 3 and 5, the AATS AODs in Fig. 9b have not been increased to account for estimated AOD below the aircraft altitude (but results for both adjusted and unadjusted AATS AODs are included in Tables 1–3). Figure 9c displays the latitudinal variation of AOD at 553 nm for the MODIS 10 km and 3 km resolution retrievals, and for mean spectrally interpolated AATS AODs before and after correction for the estimated AOD (~ 0.02) below the aircraft. AATS AODs significantly exceeded MODIS retrievals at both resolutions over most of the flight track. In fact, the difference between MODIS AODs and AATS AODs adjusted for the below-aircraft amount was 0.08–0.15 in 8 of 12 10 km grid cells. All MODIS retrievals yield a retrieval QF of 3 (very good), and used a moderate-absorption fine-mode aerosol. Figure 9d compares the MODIS 3 km and 10 km retrievals, with an R^2 of 0.90, a mean difference ~ 0 (−0.1 %), and an RMS difference of 0.02 (14 %). Figure 9e compares the 553 nm AATS (corrected for below-aircraft AOD) and MODIS AODs shown in Fig. 9d. Not surprisingly, values of R^2 are low (0.27 for 10 km and 0.14 for 3 km), and MODIS-minus-AATS mean differences (−0.06/$\sim$ −27 %) and RMS differences (0.08/ $\sim$ 36 %) are large. Despite the relatively large MODIS/AATS AOD differences, 50 % of the MODIS 10 km retrievals and 59 % of the 3 km retrievals fall within the MODIS EE. The remainder underestimate AATS AOD by greater than the EE.

Figure 10 presents an analogous set of plots for the AATS/MODIS AOD comparison for the Aqua overflight at 20.33 UT. AATS data were acquired within 22 3 km and six 10 km MODIS grid cells, although the majority of AATS measurements were taken

ACPD
13, 15007–15059, 2013

within the four 10 km cells centered east of 112.4° W, as shown in Fig. 10a. MODIS AODs underestimate the adjusted AATS values by ∼ 0.08 within the two easternmost 10 km cells and within nine 3 km cells centered between longitudes 112–112.4° W. MODIS retrievals agree with the mean of the adjusted AATS values to within the EE in 83 % (5 of 6) of 10 km grid cells and 73 % (16 of 22) of 3 km grid cells. MODIS AODs underestimate AATS values by greater than the EE in the remainder of the grid cells. The correlation (R^2 = 0.82) between the MODIS 3 km and 10 km AOD retrievals is slightly poorer, the mean difference the same, and the RMS difference slightly smaller (0.015 vs. 0.022) than for the MODIS Terra overpass in the same general region about three hours earlier. The MODIS/AATS AOD comparisons for the 10 km and 3 km retrievals exhibit no correlation (R^2 < 0.01), with mean difference values of ∼ −0.035 (−15 %) that are about 40 % smaller than the corresponding AATS/MODIS Terra negative differences (∼ −0.06/−27 %), and RMS differences of 0.047 (21 %) and 0.060 (27 %) that are 42 % and 29 % less than the AATS/MODIS Terra values. The lack of AATS-MODIS correlation is expected because the spatial variation in AATS AOD is small compared to the MODIS uncertainty. As is the case for the MODIS Terra retrievals, all MODIS Aqua retrievals yield a retrieval QF = 3 and used a moderate-absorption fine-mode aerosol. We can think of two reasons why the Terra retrieval underestimates of AATS AODs might exceed the Aqua underestimates. First, by 2008, Terra measurements were subject to sensor calibration drift (Levy et al., 2010) that led to retrievals that not only underestimate the true AOD, but are also less than the corresponding Aqua AOD retrievals by up to ∼ 0.02, which (perhaps coincidentally) is very close to the 0.026 difference between the 10 km resolution Terra MODIS-AATS AOD mean difference (−0.060) and the Aqua MODIS-AATS AOD mean difference (−0.034). However, a more likely explanation, not only for the differences between the magnitudes of the Terra and Aqua underestimates of AATS AOD, but also for the Terra and Aqua underestimates of AATS AOD, is local variability in surface properties and subsequent deviation from modeled spectral relationships not accounted for by the MODIS retrieval algorithm.

ACPD
13, 15007–15059, 2013

3.5 9 July 2008

On 9 July the P-3 flew along a south-north track over southeastern Yukon Territory during the time period 19.515–19.713 UT just prior to a MODIS Aqua overpass at 19.75 UT. Figure 11 overlays the locations of the P-3 flight track and the MODIS 10 km AOD retrieval grid cells on the MODIS RGB image. The flight included a descent from 600 to 120 m a.g.l. from 19.51 to 19.55 UT during the brief westward and southward portion of the track, followed by a turn to the north and a general S–N transect at relatively constant altitude (148 ± 21 m a.g.l.) from 19.55 to 19.69 UT, and finally an ascent to ∼ 580 m a.g.l. from 19.69 to 19.71 UT. The region was dominated by smoke and scattered clouds above the aircraft, both evident in Fig. 11.

Figure 12 examines the MODIS and AATS AODs in detail, and is analogous to Figs. 3, 9 and 10. Figure 12a overlays the P-3 flight track color-coded by the AATS 520 nm AOD on the MODIS 10 km and 3 km grid cells. The MODIS operational retrieval algorithm yielded AOD in nine intersecting 10 km cells along the P-3 track, but only eight intersecting 3 km cells (green). Missing data points along the flight track reflect AATS measurements that have been excluded by the AATS cloud filter. The red number in each 10 km cell indicates the MODIS retrieval QF, with only three very good (= 3) and two good (= 2) retrievals among the nine 10 km retrievals. Figure 12b overplots the corresponding AOD spectra (arranged in chronological order). MODIS AOD retrievals for the aerosol cloud mask off and for the cloud and NDVI masks off are not shown, but these are given in Table 1; values are little different from the operational retrievals.

As shown in Fig. 12c, the magnitude of the estimated AOD below the aircraft is almost negligible. The agreement between MODIS and AATS 553 nm AOD is better than for the 2 July smoke/cloud case, with much smaller mean percentage differences (12 % for all QF, 3 % for QF = 3) and RMS differences (3 %, 18 %) than for the 2 July case. These smaller differences combine with the greater spatial variability on 9 July to produce larger R^2 values of 0.54 and 0.73 for the 10 km and 3 km comparisons, respectively. MODIS AODs agree with the mean of the adjusted AATS values to within

ACPD
13, 15007–15059, 2013

the EE in all eight 3 km grid cells, but in only four of nine 10 km grid cells for all QF and in one of three 10 km cells with QF = 3. The two 10 km cells exhibiting the largest disagreement are the two southeastern-most cells, with locations and AOD spectra plotted in light blue (cell 1) and light green (cell 4) in Fig. 12a and b. There appears to be no correlation between the level of MODIS/AATS AOD agreement and the MODIS retrieval QF. The QF is marginal (= 1) in cells 1 and 4. The locations of the only retrieval with a QF of bad (= 0) and the remaining retrieval with a QF of marginal are the two southernmost cells (cells 2 and 3), and the MODIS AODs (0.27) agree well with AATS values (0.25) in these cells. In two (cells 5 and 6) of the three cells that yield a QF of very good (= 3), MODIS AOD overestimates the AATS AOD by 0.14 and 0.15, respectively, but these values are approximately equal to the maximum expected MODIS EE. This level of disagreement can likely be explained by spatial sampling differences within the MODIS grid cells.

3.6 Composite results for AOD and Ångström exponents

In this section we compare MODIS and AATS AOD (553 nm) and AE after aggregating the corresponding values for the five individual cases. We consider only the standard (cloud mask on) MODIS retrievals, which total 134 3 km and 58 10 km resolution data points. Figure 13a displays composite AOD before increasing the AATS values by the below-aircraft AOD estimates, and Fig. 13b presents the analogous results after adjusting the AATS AOD. Table 2 lists the statistics for the scatterplots. The agreement between MODIS 10 km retrievals and AATS AOD degrades significantly when the AATS values are increased to include the estimated AOD below the aircraft, as evidenced by larger mean and RMS differences, and by the fraction of MODIS AODs that fall within the EE. With the exception of R^2, which actually increases after adjustment of the AATS AODs, measures of the agreement between the AATS and MODIS 3 km AOD also worsen, although the degradation of the other statistics is somewhat less than for the 10 km comparison. Because some of the estimates of the below-aircraft AOD for the 2 July case are large and somewhat suspect (e.g., the smoke plume penetrated by

ACPD
13, 15007–15059, 2013

the P-3 may not have reached the ground, as the adjustment assumes; see Sect. 3.3), we present Fig. 13c and d, which are analogous to Fig. 13a and b except that they exclude all 2 July data. This reduces the number of data points to 109 and 40, respectively, for the 3 km and 10 km comparisons. The agreement improves dramatically for the 3 km and the 10 km comparisons, as evidenced by improvement in all four statistical parameters. However, the improvement in Fig. 13c's parameters over Fig. 13a's cannot be attributed to excluding the below-aircraft AOD adjustment, since neither Fig. 13c nor a uses this adjustment. Instead, the improvement might be attributed to eliminating the 2 July strong plume itself, which increases the challenge of spatiotemporal coincidence between the AATS and MODIS measurements. Examination of the statistical parameters for the reduced data set MODIS/AATS comparisons with and without adjustment of the AATS AODs for the estimated below-aircraft AOD indicates slightly worse agreement after adjustment of the AATS AODs. Finally, we note that the magnitudes of the statistical parameters for the reduced data set MODIS/AATS AOD comparisons are nearly equal for the MODIS retrievals at 3 km and 10 km resolution.

In Fig. 14, we present scatterplots of MODIS and AATS AE for the MODIS/AATS comparisons for the composite data sets at both MODIS retrieval resolutions. As noted in Sect. 2.1, MODIS AE were calculated from AOD in the three shortest MODIS wavelengths (466, 553, and 645 nm), and AATS AE were calculated from AOD in the five AATS channels centered between 451 nm and 675 nm. Results are shown for AATS data points with and without addition of the below-aircraft AOD estimate. The agreement between the MODIS and AATS AE is poor for the individual cases (not shown) and for the aggregated data. There is no improvement if the 2 July data points are omitted (not shown). This is consistent with the finding of Levy et al. (2010) that AE values in the over-land data set have little physical validity, instead primarily reflecting algorithm assumptions about particle type.

ACPD
13, 15007–15059, 2013

4 Discussion and conclusions

We have compared MODIS Collection 6 over-land AOD retrievals at 10 km and 3 km resolution with AOD calculated from coincident or near-coincident measurements acquired by AATS-14 during the summer 2008 ARCTAS field experiment. Results have been presented for five satellite overpasses that occurred during P3/AATS flights on four days. The region sampled during the 30 June event was marked by a well-defined smoke plume in an otherwise clear sky. Smoke and smoke beneath clouds pervaded the 2 and 9 July sampling regions. Data were obtained in the same general location during separate Terra and Aqua overpasses on 3 July under conditions of regionally homogeneous low AOD from smoke outflow with no distinguishable plume. Our analysis leads to the following conclusions:

1. The MODIS standard operational algorithm (i.e., with aerosol cloud mask and NDVI mask) at 10 km and at 3 km resolution retrieves the 30 June plume AOD along the P-3/AATS track with overall success, in that MODIS-AATS AOD differences are less than MODIS EE in 77 % of the 10 km grid cells and 88 % of the 3 km grid cells. However, the algorithm fails to yield an AOD retrieval within three 3 km grid cells inside the plume along the P-3 track, and within several 10 km and 3 km grid cells encompassing the plume outside the P-3 track. Both the aerosol cloud mask and the NDVI test contribute to these failures, and turning off these masks produces MODIS plume retrievals that are more complete spatially. The 3 km AODs are noisier than the 10 km values.

2. For the clear-sky 3 July coincidences, MODIS AOD retrievals agree with AATS values to within EE in 50 % of the 10 km and 59 % of the 3 km Terra retrieval grid cells, and in 83 % of the 10 km and 73 % of the 3 km Aqua grid cells. MODIS retrievals underestimate the AATS AODs by more than the EE in the remaining grid cells.

ACPD
13, 15007–15059, 2013

3. Clouds confounded the MODIS/AATS AOD comparisons on 2 and 9 July. On 2 July, clouds significantly impaired the capability of the MODIS standard retrieval algorithm to retrieve AOD along the P-3 flight track. The cloud mask's rejection of 0.5 km pixels that contained both smoke and cloud led to large underestimates of AATS AODs in those grid cells where AOD was retrieved. On 9 July, when the P-3 flight track was much shorter than that on 2 July, the algorithm retrieved AOD at 10 km resolution along most of the flight track, but only four of nine retrievals for all values of QF and only one of three retrievals with QF = 3 fall within the EE. There was no apparent correlation between the level of MODIS/AATS AOD agreement and the MODIS quality flag. There were only eight 3 km resolution retrievals, all of which had QF = 3. For these eight, all MODIS-AATS differences fall within the MODIS EE.

4. When the MODIS-AATS comparisons for the five cases are combined, 60 % of all MODIS-AATS differences for MODIS QF = 3 fall within the MODIS EE for the 10 km retrievals, and 69 % for the 3 km retrievals. If the 2 July results are excluded, these values increase to 65 % and 74 %, respectively, and values of R^2, mean difference, and RMSD increase dramatically.

5. Calculated values of MODIS and AATS AEs show no correlation. This is consistent with Levy et al. (2010), who concluded that there is no information on particle size in the MODIS over-land aerosol retrievals.

We conclude with several points considered in relation to this paper's overall purpose, which has been to compare the MODIS 3 km and 10 km resolution AOD retrievals with independent measurements by an airborne instrument, AATS, that is well suited to describing the fine spatiotemporal structure of the smoke plumes and clouds that were prevalent in ARCTAS. The comparisons in the tables and illustrations have helped to show the relative strengths and weaknesses of the 10 km and 3 km retrievals, i.e., the 3 km retrievals can depict finer horizontal structure, albeit at the price of "noisier" results (i.e., with larger EE values and AOD differences from AATS). Hence, we recommend

ACPD
13, 15007–15059, 2013

that, consistent with Collection 6, future MODIS data archives include products at both resolutions, so that data users can choose which product or products are best suited to their needs. The 30 June case has also illustrated that both the MODIS aerosol cloud mask and the NDVI mask can eliminate pixels that contain useful information on strong smoke plumes. Turning off those masks produced a more spatially complete MODIS data set in that case. These results lay the foundation for exploring whether different thresholds on cloud and NDVI masks can expand the MODIS aerosol data set in ARCTAS-like conditions of smoke plumes and clouds, without paying too high a price in contamination by clouds and highly reflecting surfaces. Potential improvements in the MODIS modeled surface spectral relationships could also be explored using AATS spectral AOD to do atmospheric correction. The current results also point to the need for analogous comparisons in different conditions (e.g., tropical biomass burning plumes and hazes, dust and urban-industrial plumes and hazes over different surface types), where different mask thresholds and surface spectral relationships may be more successful.

Acknowledgements. The ARCTAS Campaign was a collaborative effort of a large number of participants with the support of multinational agencies. Funding for the AATS measurements, and for the AATS-MODIS comparisons presented here, was provided by the NASA Radiation Sciences Program.

References

Ackerman, S. A., Strabala, K. L., Menzel, W. P., Frey, R. A., Moeller, C. C., and Gumley, L. E.: Discriminating clear sky from clouds with MODIS, J. Geophys. Res.-Atmos., 103, 32141–32157, 1998.

Anderson, T. L., Covert, D. S., Marshall, S. F., Laucks, M. L., Charlson, R. J., Waggoner, A. P., Ogren, J. A., Caldow, R., Holm, R. L., Quant, F. R., Sem, G. J., Wiedensohler, A., Ahlquist, N. A., and Bates, T. S.: Performance characteristics of a high-sensitivity, three-wavelength, total scatter/backscatter nephelometer, J. Atmos. Ocean. Tech., 13, 967–986, 1996.

ACPD
13, 15007–15059, 2013

Anderson, T. L., Charlson, R. J., Winder, D. M., Ogren, J. A., and Homen, K.: Mesoscale variations of tropospheric aerosols, J. Atmos. Sci., 60, 119–136, 2003.

Chu, D. A., Kaufman, Y. J., Ichoku, C., Remer, L. A., Tanré, D., and Holben, B. N.: Validation of MODIS aerosol optical depth retrieval over land, Geophys. Res. Lett., 29, MOD 2, 1–4, doi:10.1029/2001GL013205, 2002.

Heintzenberg, J. and Charlson, R. J.: Design and application of the integrating nephelometer: a review, J. Atmos. Ocean. Tech., 13, 987–1000, 1996.

Holben, B. N., Eck, T. F., Slutsker, I., Tanre, D., Buis, J. P., Setzer, A., Vermote, E., Reagan, J. A., Kaufman, Y. J., Nakajima, T., Lavenu, F., Jankowiak, I., and Smirnov, A.: AERONET – a federated instrument network and data archive for aerosol characterization, Remote Sens. Environ., 66, 1–16, 1998.

Jacob, D. J., Crawford, J. H., Maring, H., Clarke, A. D., Dibb, J. E., Emmons, L. K., Ferrare, R. A., Hostetler, C. A., Russell, P. B., Singh, H. B., Thompson, A. M., Shaw, G. E., McCauley, E., Pederson, J. R., and Fisher, J. A.: The Arctic Research of the Composition of the Troposphere from Aircraft and Satellites (ARCTAS) mission: design, execution, and first results, Atmos. Chem. Phys., 10, 5191–5212, doi:10.5194/acp-10-5191-2010, 2010.

Kaufman, Y. J., Tanre, D., Remer, L., Vermote, E., Chu, A., and Holben, B. N.: Operational remote sensing of tropospheric aerosol over land from EOS moderate resolution imaging spectroradiometer, J. Geophys. Res.-Atmos., 102, 17051–17067, 1997.

King, M. D., Menzel, W. P., Kaufman, Y. J., Tanre, D., Gao, B.-C., Platnick, S., Ackerman, S. A., Remer, L. A., Pincus, R., and Hubanks, P. A.: Cloud and aerosol properties, precipitable water, and profiles of temperature and humidity form MODIS, IEEE T. Geosci. Remote, 41, 442–458, 1992.

Kleidman, R. G., Smirnov, A., Levy, R.C, Mattoo, S., and Tanré, D.: Evaluation and wind speed dependence of MODIS aerosol retrievals over open ocean, IEEE T. Geosci. Remote, 50, 429–435, doi:10.1109/TGRS.2011.2162073, 2012.

Levy, R. C., Remer, L. A., Martins, J. V., Kaufman, Y. J., Plana-Fattori, A., Redemann, J., and Wenny, B.: Evaluation of the MODIS aerosol retrievals over ocean and land during CLAMS, J. Atmos. Sci., 62, 974–992, doi:10.1175/JAS3391.1, 2005.

Levy., R. C., Remer, L. A., and Dubovik, O.: Global aerosol optical properties and application to moderate resolution imaging spectroradiometer aerosol retrieval over land, J. Geophys. Res., 112, D13210, doi:10.1029/2006JD007815, 2007a.

ACPD
13, 15007–15059, 2013

Levy, R. C., Remer, L. A., Mattoo, S., Vermote, E. F., and Kaufman, Y. J.: Second-generation operational algorithm: retrieval of aerosol properties over land from inversion of moderate resolution imaging spectroradiometer spectral reflectance, J. Geophys. Res., 112, D13211, doi:10.1029/2006JD007811, 2007b.

Levy, R. C., Remer, L., Tanre, D., Mattoo, S., and Kaugman, Y.: Algorithm for remote sensing of tropospheric aerosol over dark targets from MODIS: Collections 005 and 051: Revision 2, February 2009, MODIS Algorithm Theoretical Basic Document, 2009.

Levy, R. C., Remer, L. A., Kleidman, R. G., Mattoo, S., Ichoku, C., Kahn, R., and Eck, T. F.: Global evaluation of the Collection 5 MODIS dark-target aerosol products over land, Atmos. Chem. Phys., 10, 10399–10420, doi:10.5194/acp-10-10399-2010, 2010.

Levy, R. C., Mattoo, S., Munchak, L. A., Remer, L. A., Sayer, A. M., and Hsu, N. C.: The Collection 6 MODIS aerosol products over land and ocean, Atmos. Meas. Tech. Discuss., 6, 159–259, doi:10.5194/amtd-6-159-2013, 2013.

Li, C., Lau, A. K.-H., Mai, J., and Chu, D. A.: Retrieval, validation, and application of the 1 km aerosol optical depth from MODIS measurements over Hong Kong, IEEE T. Geosci. Remote, 43, 2650–2658, 2005.

Li, R., Remer, L., Kaufman, Y., Mattoo, S., Gao, B., and Vermote, E.: Snow and ice mask for the MODIS aerosol products, IEEE T. Geosci. Remote, 2, 306–310, 2005.

Livingston, J. M., Russell, P. B., Reid, J. S., Redemann, J., Schmid, B., Allen, D. A., Torres, O., Levy, R. C., Remer, L. A., Holben, B. N., Smirnov, A., Dubovik, O., Welton, E. J., Campbell, J. R., Wang, J., and Christopher, S. A.: Airborne sunphotometer measurements of aerosol optical depth and columnar water vapor during the Puerto Rico Dust Experiment and comparison with land, aircraft, and satellite measurements, J. Geophys. Res., 108, 8588, doi:10.1029/2002JD002520, 2003.

Livingston, J. M., Schmid, B., Russell, P. B., Eilers, J. A., Kolyer, R. W., Redemann, J., Ramirez, S. R., Yee, J.-H., Swartz, W. H., Trepte, C. R., Thomason, L. W., Pitts, M. C., Avery, M. A., Randall, C. E., Lumpe, J. D., Bevilacqua, R. M., Bittner, M., Erbertseder, T., McPeters, R. D., Shetter, R. E., Browell, E. V., Kerr, J. B., and Lamb, K.: Retrieval of ozone column content from airborne Sun photometer measurements during SOLVE II: comparison with coincident satellite and aircraft measurements, Atmos. Chem. Phys., 5, 2035–2054, doi:10.5194/acp-5-2035-2005, 2005.

Livingston, J. M., Schmid, B., Redemann, J., Russell, P. B., Ramirez, S. A., Eilers, J., Gore, W., Howard, S., Pommier, J., Fetzer, E. J., Seemann, S. W., Borbas, E., Wolfe, D. E., and

ACPD
13, 15007–15059, 2013

Thompson, A. M.: Comparison of water vapor measurements by airborne sunphotometer and near-coincident in situ and satellite sensors during INTEX/ITCT 2004, J. Geophys. Res., 112, D12S16, doi:10.1029/2006JD007733, 2007.

Livingston, J. M., Redemann, J., Russell, P. B., Torres, O., Veihelmann, B., Veefkind, P., Braak, R., Smirnov, A., Remer, L., Bergstrom, R. W., Coddington, O., Schmidt, K. S., Pilewskie, P., Johnson, R., and Zhang, Q.: Comparison of aerosol optical depths from the Ozone Monitoring Instrument (OMI) on Aura with results from airborne sunphotometry, other space and ground measurements during MILAGRO/INTEX-B, Atmos. Chem. Phys., 9, 6743–6765, doi:10.5194/acp-9-6743-2009, 2009.

Martins, J. V., Tanré, D., Remer, L. A., Kaufman, Y. J., Mattoo, S., and Levy, R.: MODIS Cloud screening for remote sensing of aerosol over oceans using spatial variability, Geophys. Res. Lett., 29, MOD 4, 1–4, doi:10.1029/2001GL013252, 2002.

Munchak, L. A., Levy, R. C., Mattoo, S., Remer, L. A., Holben, B. N., Schafer, J. S., Hostetler, C. A., and Ferrare, R. A.: MODIS 3 km aerosol product: applications over land in an urban/suburban region, Atmos. Meas. Tech. Discuss., 6, 1683–1716, doi:10.5194/amtd-6-1683-2013, 2013.

Redemann, J., Schmid, B., Eilers, J. A., Kahn, R. A., Levy, R. C., Russell, P. B., Livingston, J. M., Hobbs, P. V., Smith Jr., W. L., and Holben, B. N.: Suborbital measurements of spectral aerosol optical depth and its variability at sub-satellite grid scales in support of CLAMS, 2001, J. Atmos. Sci., 62, 933–1007, doi:10.1175/JAS3387.1, 2005.

Redemann, J., Zhang, Q., Schmid, B., Russell, P. B., Livingston, J. M., Jonsson, H., and Remer, L. A.: Assessment of MODIS-derived visible and near-IR aerosol optical properties and their spatial variability in the presence of mineral dust, Geophys. Res. Lett., 33, L18814, doi:10.1029/2006GL026626, 2006.

Remer, L. A., Tanré, D., Kaufman, Y. J., Ichoku, C., Mattoo, S., Levy., R., Chu, D. A., Holben, B. N., Dubovik, O., Smirnov, A., Martins, J. V., Li, R.-R., Ichoku, C., and Ahmad, Z.: Validation of MODIS aerosol retrieval over ocean, Geophys. Res. Lett., 29, MOD 3, 1–4, doi:10.1029/2001GL013204, 2002.

Remer, L. A., Kaufman, Y. J., Tanré, D., Mattoo, S., Chu, D. A., Martins, J. V., Li, R.-R., Ichoku, C., Levy, R. C., Kleidman, R. G., Eck, T. F., Vermote, E., and Holben, B. N.: The MODIS aerosol algorithm, products and validation, J. Atmos. Sci., 62, 947–973, 2005.

ACPD
13, 15007–15059, 2013

Remer, L. A., Mattoo, S., Levy, R. C., Heidinger, A., Pierce, R. B., and Chin, M.: Retrieving aerosol in a cloudy environment: aerosol product availability as a function of spatial resolution, Atmos. Meas. Tech., 5, 1823–1840, doi:10.5194/amt-5-1823-2012, 2012.

Remer, L. A., Mattoo, S., Levy, R. C., and Munchak, L.: MODIS 3 km aerosol product: algorithm and global perspective, Atmos. Meas. Tech. Discuss., 6, 69–112, doi:10.5194/amtd-6-69-2013, 2013.

Russell, P. B., Livingston, J. M., Dutton, E. G., Pueschel, R. F., Regan, J. A., DeFoor, T. E., Box, M. A., Allen, D., Pilewskie, P., Herman, B. M., Kinne, S. A., and Hofmann, D. J.: Pinatubo and pre-Pinatubo optical depth spectra: Mauna Loa measurements, comparisons, inferred particle size distributions, radiative effects, and relationship to lidar data, J. Geophys. Res., 98, 22969–22985, 1993a.

Russell, P. B., Livingston, J. M., Pueschel, R. F., Reagan, J. A., Browell, E. V., Toon, G. C., Newman, P. A., Schoeberl, M. R., Lait, L. R., Pfister, L., Gao, Q., and Herman, B. M.: Post-Pinatubo optical depth spectra vs. latitude and vortex structure: Airborne tracking sunphotometer measurements in AASE II, Geophys. Res. Lett., 20, 2571–2574, 1993b.

Russell, P., Livingston, J., Schmid, B., Eilers, J., Kolyer, R., Redemann, J., Ramirez, S., Yee, J.-H., Swartz, W., Shetter, R., Trepte, C., Risley Jr., A., Wenny, B., Zawodny, J., Chu, W., Pitts, M., Lumpe, J., Fromm, M., Randall, C., Hoppel, K., and Bevilacqua, R.: Aerosol optical depth measurements by airborne sun photometer in SOLVE II: Comparisons to SAGE III, POAM III and airborne spectrometer measurements, Atmos. Chem. Phys., 5, 1311–1339, doi:10.5194/acp-5-1311-2005, 2005.

Russell, P. B., Livingston, J. M., Redemann, J., Schmid, B., Ramirez, S. A., Eilers, J., Kahn, R., Chu, A., Remer, L., Quinn, P. K., Rood, M. J., and Wang, W.: Multi-grid-cell validation of satellite aerosol property retrievals in INTEX/ITCT/ICARTT 2004, J. Geophys. Res., 112, D12S09, doi:10.1029/2006JD007606, 2007.

Schmid, B. and Wehrli, C.: Comparison of sun photometer calibration by Langley technique and standard lamp, Appl. Optics, 34, 4500–4512, 1995.

Schmid, B., Thome, K. J., Demoulin, P., Peter, R., Matzler, C., and Sekler, J.: Comparison of modeled and empirical approaches for retrieving columnar water vapor from solar transmittance measurements in the 0.94 µm region, J. Geophys. Res., 101, 9345–9358, 1996.

Schmid, B., Spyak, P. R., Biggar, S. F., Wehrli, C., Sekler, J., Ingold, T., Mätzler, C., Kämpfer, N.: Evaluation of the applicability of solar and lamp radiometric calibrations of a precision sunphotometer operating between 300 and 1025 nm, Appl. Optics, 37, 3923–3941, 1998.

ACPD
13, 15007–15059, 2013

Schmid, B., Michalsky, J. J., Slater, D. W., Barnard, J. C., Halthore, R. N., Liljegren, J. C., Holben, B. N., Eck, T. F., Livingston, J. M., Russell, P. B., Ingold, T., and Slutsker, I.: Comparison of columnar water-vapor measurements from solar transmittance methods, Appl. Optics, 40, 1886–1896, 2001.

Schmid, B., Hegg, D. A., Wang, J., Bates, D., Redemann, J., Russell, P. B., Livingston, J. M., Jonsson, H. H., Welton, E. J., Deinfeld, J. H., Flagan, R. C., Covert, D. S., Dubovik, O., and Jefferson, A.: Column closure studies of lower tropospheric aerosol and water vapor during ACE-Asia using airborne sunphotometer and airborne in situ and ship-based lidar measurements, J. Geophys. Res., 108, 8656, doi:10.1029/2002JD003361, 2003a.

Schmid, B., Redemann, J., Russell, P. B., Hobbs, P. V., Hlavka, D. L., McGill, M. J., Holben, B. N., Welton, E. J., Campbell, J. R., Torres, O., Kahn, R. A., Diner, D. J., Helmlinger, M. C., Chu, D. A., Robles-Gonzales, C., and de Leeuw, G.: Coordinated airborne, spaceborne, and ground-based measurements of massive thick aerosol layers during the dry season in Southern Africa, J. Geophys. Res., 108, 8496, doi:10.1029/2002JD002297, 2003b.

Segal-Rosenheimer, M., Russell, P. B., Livingston, J. M., Ramachandran, S., Redemann, J., and Baum, B. A.: Retrieval of cirrus properties by Sun photometry: A new perspective on an old issue, J. Geophys. Res.-Atmos., 118, doi:10.1002/jgrd.50185, 2013.

Shinozuka, Y. and Redemann, J.: Horizontal variability of aerosol optical depth observed during the ARCTAS airborne experiment, Atmos. Chem. Phys., 11, 8489–8495, doi:10.5194/acp-11-8489-2011, 2011.

Shinozuka, Y., Redemann, J., Livingston, J. M., Russell, P. B., Clarke, A. D., Howell, S. G., Freitag, S., O'Neill, N. T., Reid, E. A., Johnson, R., Ramachandran, S., McNaughton, C. S., Kapustin, V. N., Brekhovskikh, V., Holben, B. N., and McArthur, L. J. B.: Airborne observation of aerosol optical depth during ARCTAS: vertical profiles, inter-comparison and fine-mode fraction, Atmos. Chem. Phys., 11, 3673–3688, doi:10.5194/acp-11-3673-2011, 2011.

ACPD
13, 15007–15059, 2013

Table 1. Parameters for individual MODIS 10 km aerosol retrieval grid cells, including MODIS and AATS AOD and Ångström Exponents.

Date (satellite)	MODIS					AATS	AOD 553 nm					Ångström Exponent			
	Cell index	Qual. flag	Number of 0.5 km pixels			No. obs	MODIS			AATS		MODIS		AATS	
	number	Masks on	Masks on	Cld msk off	+NDVI off	In cell	Masks on	Cld off	+NDVI off	Unadj	Adj	Masks on	Cld off	Unadj	Adj
30 Jun (Aqua)	1	3	62	112	114	14	0.092	0.106	0.105	0.056	0.061	1.734	1.739	1.629	1.659
	2	3	82	115	119	19	0.012	0.020	0.020	0.055	0.059	1.881	1.739	1.626	1.670
	3	3	83	109	111	19	0.028	0.031	0.035	0.056	0.059	1.676	1.781	1.613	1.648
	4	3	95	115	115	20	0.160	0.162	0.162	0.066	0.076	0.619	0.595	1.725	1.754
	5	3	115	118	120	18	0.041	0.042	0.041	0.045	0.048	1.793	1.802	1.557	1.587
	6	3	111	116	118	20	0.110	0.107	0.105	0.106	0.123	0.928	1.412	1.970	2.008
	7	3	64	103	118	19	1.189	1.084	1.114	1.167	1.239	1.256	1.191	2.156	2.166
	8	3	102	118	121	20	1.039	1.022	1.026	0.864	0.982	0.625	0.627	2.146	2.160
	9	3	105	109	117	16	0.152	0.162	0.182	0.328	0.402	1.736	1.755	2.115	2.137
	10	3	109	116	121	15	0.026	0.030	0.028	0.065	0.080	1.738	1.842	1.775	1.833
	11	3	107	107	113	2	0.018	0.018	0.016	0.040	0.044	1.935	1.935	1.551	1.586
	12	3	106	106	112	18	0.031	0.031	0.037	0.041	0.045	1.781	1.781	1.584	1.627
	13	3	100	100	109	18	0.047	0.047	0.055	0.042	0.046	1.785	1.785	1.628	1.656
2 Jul (Aqua)	1			46	121	47		1.817	2.076	1.711	2.964		1.235	1.857	1.896
	2			52	121	46		0.690	1.117	1.438	2.219		1.253	2.003	1.986
	3	3	95	98	118	48	0.115	0.115	0.122	0.089	0.148	1.762	1.727	1.419	1.550
	4	0	17	54	61	28	0.088	0.112	0.113	0.050	0.062	1.744	1.754	1.125	1.275
	5	3	46	93	112	9	0.096	0.095	0.097	0.051	0.064	1.748	1.743	1.099	1.229
	6			41	61	16		1.272	1.187	0.628	1.117		1.406	1.420	1.575
	7	2	33	82	88	14	0.282	0.257	0.267	0.183	0.257	1.726	1.735	1.239	1.376
	8			42	48	10		0.292	0.297	0.269	0.415		0.828	1.099	1.302
	9			42	50	9		0.926	0.939	0.315	0.505		1.516	1.544	1.621
	10			27	67	13		0.692	0.574	0.761	1.151		1.601	1.788	1.826
	11			16	42	3		1.820	1.880	0.960	1.527		1.233	1.921	1.992
	12			17	57	12		1.154	1.654	0.721	1.196		1.442	1.999	2.080
	13			24	51	7		0.275	0.287	0.156	0.312		1.740	1.675	1.887
	14			21	34	10		0.253	0.247	0.076	0.096		1.730	1.420	1.543
	15			16	25	2		0.245	0.295	0.065	0.083		1.737	1.412	1.500
	16	2	40	75	109	11	0.144	0.169	0.183	0.266	1.318	1.748	1.731	1.496	1.864
	17	1	27	63	119	1	0.165	0.188	0.391	0.926	2.164	0.620	0.608	1.776	1.783
	18			53	115	20		0.438	0.829	1.819	2.715		1.685	1.880	1.884
	19			21	119	23		0.833	2.403	1.701	2.701		1.323	2.083	2.047
	20	3	55	96	121	20	0.727	0.816	0.857	0.791	1.338	1.583	1.557	1.579	1.691
	21	3	104	114	121	20	0.387	0.386	0.387	0.331	0.621	1.696	1.700	1.423	1.495
	22	2	39	45	49	7	0.368	0.369	0.371	0.258	0.451	0.580	0.578	1.260	1.291
	23	0	73	86	121	14	0.535	0.535	0.553	0.233	0.429	0.545	0.546	1.163	1.225
	24	2	46	69	121	23	0.333	0.319	0.350	0.269	0.454	1.707	1.718	0.980	1.062
	25	0	30	107	119	35	0.267	0.342	0.356	0.336	0.495	1.739	1.716	1.001	1.073
	26	0	24	110	118	15	0.438	0.605	0.611	0.366	0.499	1.685	1.631	1.459	1.493
	27	2	46	83	121	14	0.167	0.185	0.193	0.295	0.442	1.739	1.736	0.973	1.083
	28	2	44	79	120	11	0.257	0.246	0.248	0.223	0.337	1.744	1.746	1.205	1.337
	29	1	22	46	59	12	0.159	0.163	0.189	0.148	0.192	0.606	1.744	1.543	1.603
	30	3	79	115	120	16	0.126	0.155	0.159	0.801	0.925	1.739	1.742	1.730	1.739
	31	3	51	99	115	7	0.373	0.511	0.516	1.776	2.003	1.705	1.663	1.822	1.829
	32			20	58	7		0.849	1.621	2.365	2.648		1.542	1.782	1.791

ACPD
13, 15007–15059, 2013

Table 1. Continued.

Date (satellite)	MODIS					AATS	AOD 553 nm					Ångström Exponent			
	Cell index number	Qual. flag Masks on	Number of 0.5 km pixels Masks on	Cld msk off	+NDVI off	No. obs In cell	MODIS Masks on	MODIS Cld off	MODIS +NDVI off	AATS Unadj	AATS Adj	MODIS Masks on	MODIS Cld off	AATS Unadj	AATS Adj
3 Jul (Terra)	1	3	117			33	0.230			0.200	0.225	0.609		1.709	1.718
	2	3	121			7	0.249			0.213	0.229	0.610		1.676	1.693
	3	3	98			20	0.171			0.219	0.236	1.746		1.675	1.684
	4	3	111			22	0.157			0.221	0.240	1.747		1.678	1.686
	5	3	120			4	0.161			0.210	0.230	1.741		1.682	1.689
	6	3	109			23	0.245			0.206	0.227	0.606		1.681	1.695
	7	3	120			25	0.107			0.196	0.217	1.759		1.691	1.709
	8	3	113			24	0.125			0.190	0.209	1.735		1.697	1.710
	9	3	121			22	0.080			0.190	0.213	1.766		1.701	1.718
	10	3	120			4	0.088			0.193	0.215	1.744		1.700	1.716
	11	3	121			25	0.115			0.192	0.214	1.743		1.706	1.717
	12	3	121			11	0.221			0.194	0.219	0.595		1.704	1.725
3 Jul (Aqua)	1	3	120			37	0.151			0.194	0.216	1.762		1.701	1.713
	2	3	117			24	0.146			0.193	0.226	1.751		1.703	1.723
	3	3	116			86	0.208			0.197	0.221	1.741		1.712	1.726
	4	3	118			11	0.189			0.199	0.223	1.732		1.718	1.736
	5	3	118			4	0.240			0.201	0.222	0.717		1.721	1.734
	6	3	120			81	0.196			0.201	0.223	1.743		1.724	1.739
9 Jul (Aqua)	1	1	24	37	70	31	0.676	0.671	0.623	0.462	0.490	0.526	0.526	1.550	1.575
	2	0	20	75	112	24	0.265	0.302	0.306	0.242	0.250	1.737	1.727	1.551	1.569
	3	1	21	92	117	58	0.272	0.318	0.312	0.247	0.253	1.405	1.504	1.554	1.568
	4	1	26	88	105	19	0.492	0.522	0.545	0.307	0.316	0.928	0.796	1.554	1.565
	5	3	62	100	120	35	0.532	0.595	0.591	0.384	0.391	0.803	0.539	1.494	1.507
	6	3	77	103	119	12	0.654	0.663	0.654	0.496	0.503	1.148	1.151	1.502	1.507
	7	2	34	73	83	38	0.711	0.751	0.735	0.683	0.696	1.142	1.136	1.460	1.471
	8	2	45	67	118	11	0.459	0.471	0.709	0.590	0.610	1.678	1.679	1.505	1.523
	9	3	94	103	121	19	0.351	0.352	0.352	0.383	0.428	1.712	1.708	1.561	1.601

ACPD
13, 15007–15059, 2013

Table 2. Summary parameters and statistics for MODIS/AATS AOD comparisons.

Date(satellite)	MODIS								AOD (MODIS – AATS)					AOD (MODIS 3 km – MODIS 10 km)				
	Cell res. [km]	Masks Cloud	Masks NDVI	Retrieval qual flag	Total no. cells	Number of cells (%) < AATS AOD	Number of cells (%) Within EE	Number of cells (%) > AATS AOD	R^2	Mean difference Abs	Mean difference Rel (%)	RMSD Abs	RMSD Rel (%)	R^2	Mean difference Abs	Mean difference Rel (%)	RMSD Abs	RMSD Rel (%)
30 Jun	10	on	on	3	13	2(15)	10(77)	1(8)	0.960	−0.025	−9.8	0.080	31.9	0.986	0.015	6.8	0.059	26.0
(Aqua)	3	on	on	3	35	2(6)	31(88)	2(6)	0.925	0.035	16.3	0.126	58.2					
2 Jul	10	on	on	all	18	9(50)	9(50)	0	0.049	−0.398	−58.5	0.718	105.9	0.885	0.025	8.9	0.065	23.1
(Aqua)	10	on	on	3,2,1	14	8(57)	6(43)	0	0.069	−0.501	−73.9	0.811	119.6	0.933	0.022	8.5	0.051	19.2
	10	on	on	3,2	12	7(58)	5(42)	0	0.183	−0.415	−61.3	0.659	97.2	0.933	0.029	10.2	0.054	19.3
	10	on	on	3	6	4(67)	2(33)	0	0.367	−0.546	−80.5	0.788	116.3	0.979	0.028	9.2	0.048	15.7
	3	on	on	all	25	12(48)	12(48)	1(4)	0.243	−0.230	−38.2	0.462	76.8					
	3	on	on	3	23	12(52)	10(43)	1(4)	0.282	−0.257	−41.8	0.480	77.9					
3 Jul	10	on	on	3	12	6(50)	6(50)	0	0.268	−0.060	−27.1	0.081	35.5	0.905	−0.0002	−0.1	0.022	13.8
(Terra)	3	on	on	3	44	18(41)	26(59)	0	0.135	−0.057	−25.8	0.084	37.8					
3 Jul	10	on	on	3	6	1(17)	5(83)	0	0.007	−0.034	−15.1	0.047	21.0	0.817	0.002	1.0	0.015	7.9
(Aqua)	3	on	on	3	22	6(27)	16(73)	0	0.003	−0.036	−16.0	0.060	26.9					
9 Jul	10	on	on	all	9	1(11)	4(44)	4(44)	0.539	0.053	12.1	0.124	28.3	0.874	0.037	7.6	0.068	13.9
(Aqua)	10	on	on	3	3	0	1(33)	2(67)	0.325	0.072	16.3	0.127	28.9	0.988	0.052	10.1	0.059	11.5
	3	on	on	3 (all = 3)	8	0	8(100)	0	0.727	0.016	2.9	0.095	17.5					
Aggregated																		
All dates	10	on	on	all	58	19(33)	34(59)	5(9)	0.235	−0.137	−33.9	0.407	100.7	0.954	0.017	6.4	0.054	20.3
	10	on	on	3	40	13(32)	24(60)	3(8)	0.472	−0.108	−31.5	0.314	91.8	0.974	0.013	5.7		
	3	on	on	all	134	38(28)	93(69)	3(2)	0.544	−0.057	−18.5	0.218	70.1					
	3	on	on	3	132	38(28)	91(69)	3(2)	0.545	−0.060	−19.3	0.219	70.8					
All except	10	on	on	all	40	10(25)	25(62)	5(13)	0.894	−0.019	−6.9	0.089	31.6	0.970	0.014	5.2	0.049	18.6
2 Jul	10	on	on	3	34	9(26)	22(65)	3(9)	0.916	−0.030	−12.0	0.081	32.2	0.976	0.011	4.8	0.043	19.3
	3	on	on	3 (all = 3)	109	26(24)	81(74)	2(2)	0.877	−0.018	−7.3	0.097	39.6					
All dates*	10	on	on	all	58	11(19)	39(67)	8(14)	0.403	−0.039	−12.8	0.244	79.9					
	10	on	on	3	40	7(18)	30(75)	3(7)	0.471	−0.056	−19.4	0.256	87.9					
	3	on	on	all	134	18(13)	105(78)	11(8)	0.515	−0.003	−1.0	0.191	74.5					
	3	on	on	3	132	18(14)	104(79)	10(8)	0.520	−0.006	−2.2	0.190	74.5					
All except	10	on	on	all	40	6(15)	29(73)	5(12)	0.908	0.003	1.0	0.084	32.6					
2 Jul*	10	on	on	3	34	5(15)	26(76)	3(9)	0.930	−0.007	−3.1	0.074	32.2					
	3	on	on	3 (all = 3)	109	14(13)	89(82)	6(5)	0.863	0.006	2.5	0.105	47.8					

* For these comparisons, AATS AOD values do *not* include estimate of AOD below aircraft.

ACPD
13, 15007–15059, 2013

Table 3. Summary parameters and statistics for MODIS/AATS Ångström Exponent comparisons.

Date (satellite)	MODIS				Ångström Exponent (MODIS – AATS)					Ångström Exponent (MODIS – Adjusted AATS)				
	Cell res. [km]	Aerosol cloud mask	Retrieval Qual flag	Total no. cells	R^2	Mean difference Abs	Mean difference Rel (%)	RMSD Abs	RMSD Rel (%)	R^2	Mean difference Abs	Mean difference Rel (%)	RMSD Abs	RMSD Rel (%)
30 Jun (Aqua)	10	on	3	13	0.339	−0.276	−15.6	0.675	38.0	0.332	−0.308	−17.1	0.683	37.8
	3	on	3	35	0.067	−0.401	−22.9	0.723	41.3	0.056	−0.435	−24.4	0.736	41.2
2 Jul (Aqua)	10	on	all	18	0.034	0.118	8.7	0.595	44.1	0.005	0.023	1.6	0.555	38.4
	3	on	all	25	0.087	0.173	12.7	0.432	31.8	0.086	0.083	5.7	0.397	27.4
	10	on	3	6	0.076	0.193	14.3	0.323	24.0	0.121	0.116	7.3	0.252	15.9
	3	on	3	23	0.087	0.173	12.7	0.432	31.8	0.102	0.058	4.0	0.399	27.3
3 Jul (Terra, Aqua)	10	on	3	18	0.001	−0.263	−15.5	0.567	33.3	0.000	−0.277	−16.2	0.574	33.5
	3	on	3	66	0.002	−0.370	−21.8	0.660	38.8	0.003	−0.384	−22.4	0.667	39.0
9 Jul (Aqua)	10	on	all	9	0.030	−0.294	−19.3	0.500	32.8	0.047	−0.312	−20.2	0.509	33.0
	10	on	3	3	0.928	−0.298	−19.5	0.457	29.9	0.860	−0.317	−20.6	0.461	29.9
	3	on	3 (all = 3)	8	0.017	−0.378	−25.2	0.583	38.8	0.044	−0.397	−26.1	0.592	38.9
Aggregated														
All dates	10	on	all	58	0.022	−0.153	−9.7	0.592	37.5	0.011	−0.196	−12.1	0.585	36.0
	3	on	all	134	0.008	−0.277	−17.0	0.637	38.9	0.005	−0.311	−18.6	0.641	38.4
	10	on	3	40	0.065	−0.201	−12.7	0.569	36.0	0.057	−0.231	−13.5	0.570	33.3
	3	on	3	132	0.008	−0.277	−17.0	0.637	38.9	0.003	−0.321	−19.2	0.644	38.4
All except 2 Jul	10	on	all	40	0.016	−0.274	−16.3	0.591	35.1	0.012	−0.295	−17.3	0.598	35.1
	10	on	3	34	0.049	−0.271	−16.1	0.602	35.7	0.041	−0.292	−16.9	0.609	35.2
	3	on	3 (all = 3)	109	0.005	−0.381	−22.4	0.675	39.7	0.003	−0.401	−23.3	0.685	39.8

ACPD
13, 15007–15059, 2013

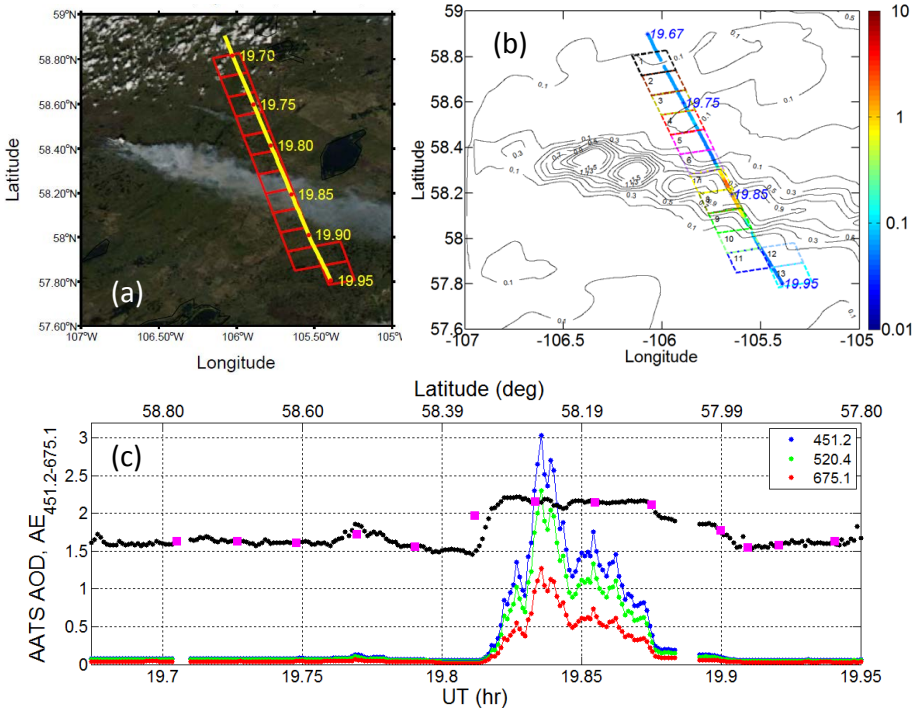

Fig. 1. (a) Aqua MODIS RGB image for the overpass at 19.85 UT on 30 June 2008. Locations of the MODIS 10 km resolution aerosol retrieval grid cells (red) and the P-3/AATS-14 flight track (yellow) are overlaid. Yellow numbers give UT along the P-3 flight track. **(b)** Overlay of MODIS grid cells (color-coded for comparison with AATS AOD spectra in Fig. 3) and P-3 track (color-coded by AATS 520 nm AOD) on contour map of MODIS AOD retrieved at 10 km resolution with the aerosol cloud mask and the NDVI mask turned off. Cells are numbered from NW to SE. **(c)** Time and latitude series of AATS AOD (colors) and Angstrom exponent (AE, black) along the P-3 flight track; magenta squares show mean AATS AE calculated for AATS measurements within individual MODIS 10 km grid cells.

ACPD
13, 15007–15059, 2013

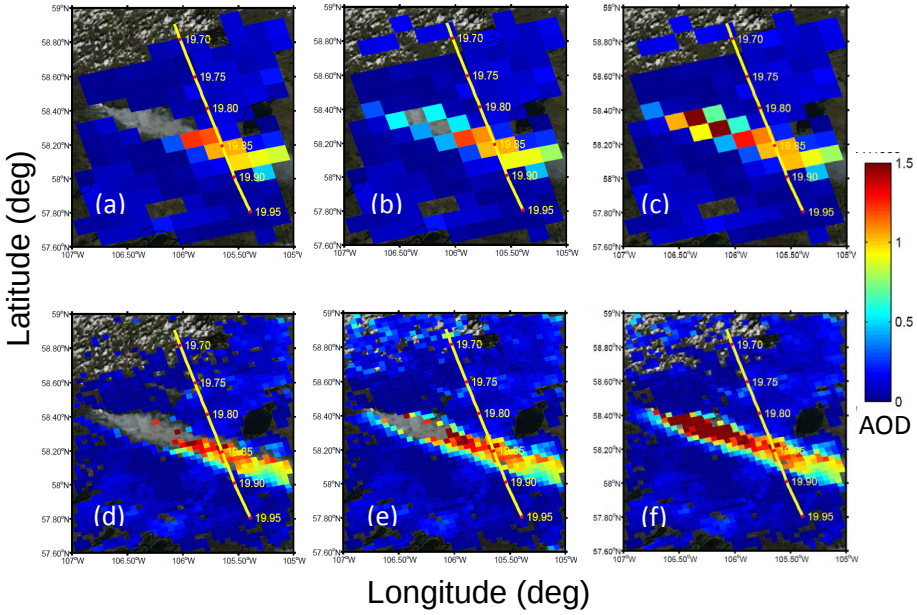

Fig. 2. Overlay of P-3 flight track and color-coded MODIS AOD retrievals at 553 nm at 10 km **(a–c)** and 3 km **(d–f)** resolution on RGB image for the 19.85 UT overpass on 30 June 2008. Results for MODIS C006 **(a, d)** operational retrieval, **(b, e)** retrieval with aerosol cloud mask off, **(c, f)** retrieval with both aerosol cloud mask and NDVI mask off.

ACPD
13, 15007–15059, 2013

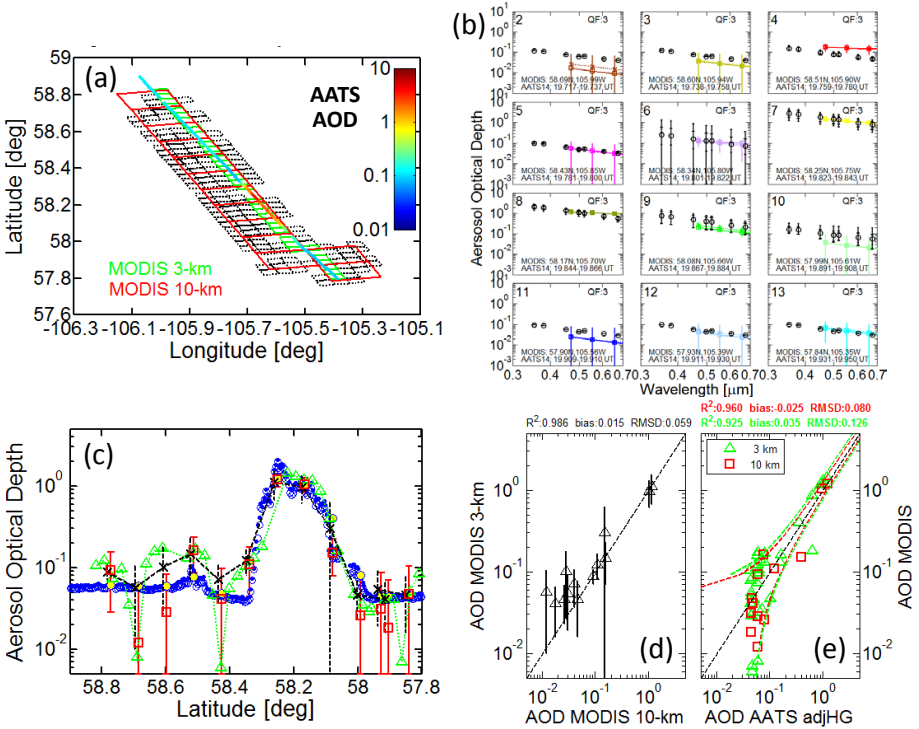

ACPD
13, 15007–15059, 2013

Comparison of MODIS 3 km and 10 km resolution

J. M. Livingston et al.

Fig. 3. Results for 30 June 2008 AATS/MODIS coincidence. **(a)** Plan view map showing overlay of P-3 flight track (color-coded by AATS 520 nm AOD), MODIS operational 10 km and 3 km retrieval grid cells intersecting the P-3 track, and MODIS 3 km (black) grid cells intersecting the 10 km grid cells. **(b)** MODIS (colored symbols and lines follow same color scheme as in Fig. 1b) and unadjusted AATS (black circles) AOD spectra within the 10 km grid cells. Cell number is given in the upper left of each frame, and the MODIS retrieval quality flag QF is listed in the upper right. The northernmost cell, Cell 1, has been omitted to maximize the display. Vertical bars on the AATS AOD points represent ± one sample standard deviation (wide ticks) and range (narrow ticks) of AOD within each cell. MODIS AOD spectra are shown for the operational retrieval (colored squares with solid line) and for the retrieval with the aerosol cloud mask and the NDVI mask off (colored x symbols with dashed line). **(c)** Latitudinal variation of 553 nm AOD for AATS (blue circles before and blue dots after addition of below-aircraft AOD estimate), for MODIS 10 km (red) and 3 km (green) operational retrievals along the P-3 track, and for mean ± one standard deviation MODIS 3 km retrievals (black) within each 10 km cell. **(d, e)** Scatterplots of the data shown in **(c)**. Dashed lines in **(e)** represent the one-to-one MODIS/adjusted AATS AOD correspondence, and ± one standard deviation boundaries of the MODIS AOD expected errors (EE, defined in text). The AATS values in **(e)** include below-aircraft AOD estimated from the HiGEAR data.

ACPD
13, 15007–15059, 2013

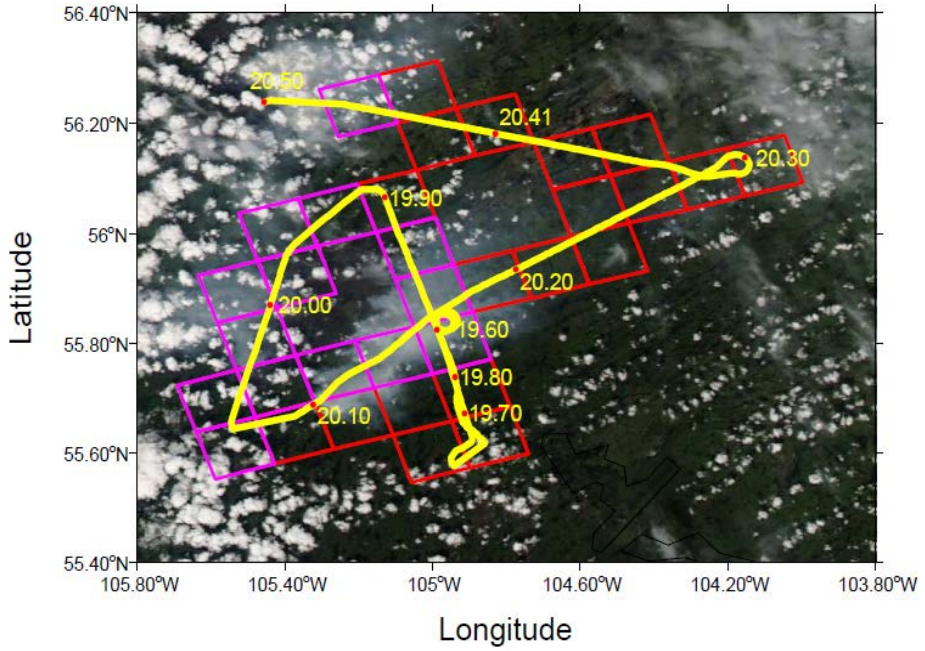

Fig. 4. Aqua MODIS RGB image for the overpass at 19.58 UT on 2 July 2008, with overlay of locations of the P-3 flight track (yellow) and the MODIS 10 km resolution aerosol retrieval grid cells (red for a retrieval with the MODIS operational algorithm, and magenta for a retrieval only for the cloud mask or the cloud and NDVI masks off).

ACPD
13, 15007–15059, 2013

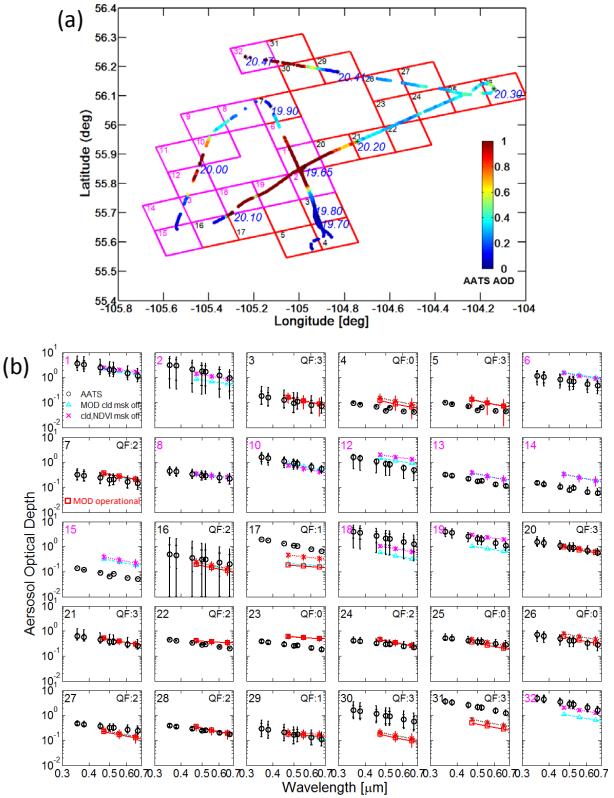

Fig. 5. For 2 July: **(a)** overlay of color-coded (by AATS 520 nm AOD) P-3 flight track and locations of the MODIS 10 km grid cells for retrievals with (red cell boundaries with black cell numbers) and without (magenta cell boundaries and numbers) the aerosol cloud mask (or the cloud and NDVI masks); **(b)** unadjusted AATS and MODIS AOD spectra. As explained in the text, retrieval quality flags are valid and shown only for MODIS operational retrievals.

ACPD
13, 15007–15059, 2013

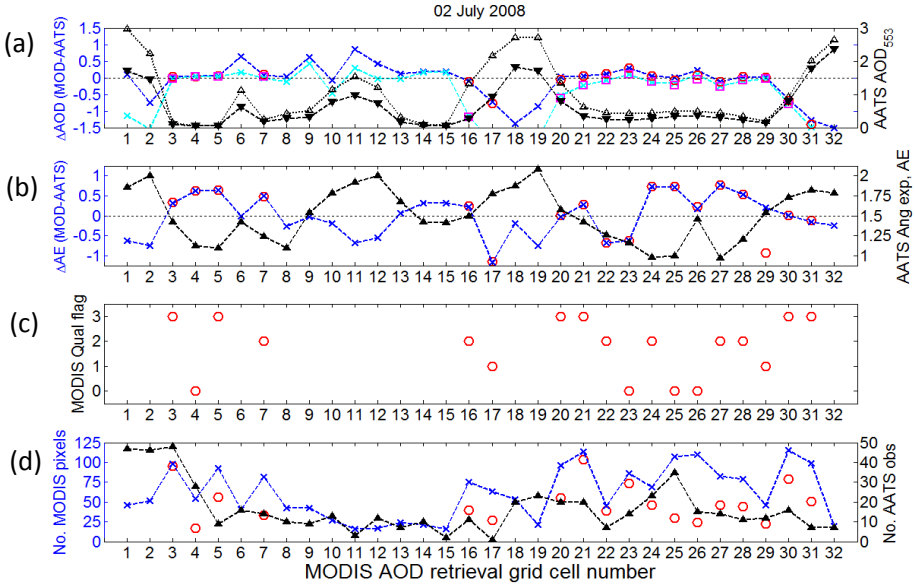

Fig. 6. For 2 July: parameters pertaining to the comparison of MODIS 10 km retrievals and AATS AOD as a function of the 10 km retrieval grid cell numbers shown in Fig. 5. **(a)** AATS AOD (right axis scale) before (black solid triangles and dashed line) and after (black open triangles and dotted line) addition of the below aircraft AOD estimates, corresponding MODIS minus AATS AOD differences (left axis scale) for the MODIS operational retrievals (red circles – unadjusted AATS AOD, magenta squares – adjusted AATS AOD) and for the special MODIS retrievals (blue Xs and dashed line – unadjusted AATS AOD, cyan Xs and dashed line – adjusted AATS AOD) with the aerosol cloud mask off. **(b)** Calculated AE values for unadjusted AATS (black, right axis scale), and MODIS minus AATS AE differences (red – MODIS operational, blue – MODIS aerosol cloud mask off, left axis scale). **(c)** MODIS quality flags for the operational retrievals. **(d)** Number of 0.5 km resolution pixels (left axis scale) used in the MODIS 10 km retrieval (red for operational retrieval, blue for retrievals with aerosol cloud mask off), and number of AATS AOD measurements (right axis scale) within each 10 km grid cell.

ACPD
13, 15007–15059, 2013

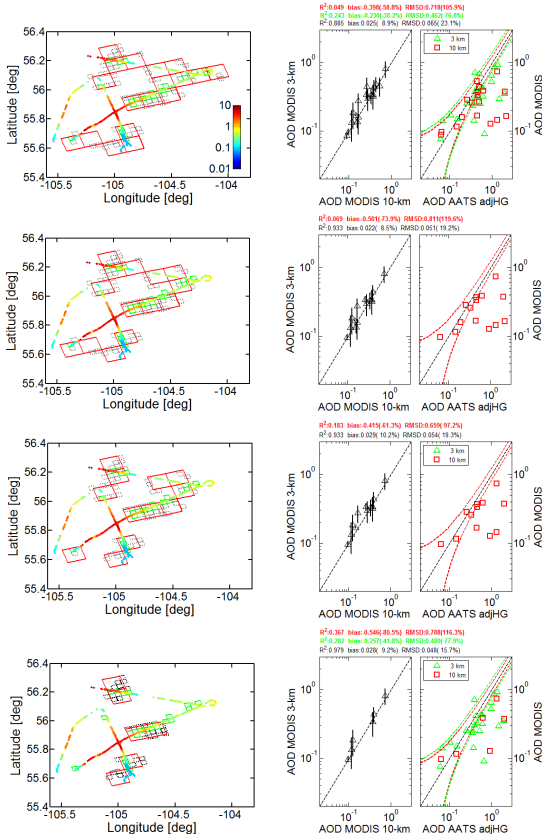

Fig. 7. For 2 July: map overlays and MODIS 3 km/10 km and MODIS/AATS AOD scatterplot results for different values of the MODIS retrieval quality flag for the MODIS operational AOD retrievals: **(a)** QF ≥ 0, **(b)** QF ≥ 1, **(c)** QF ≥ 2, **(d)** QF = 3. Retrievals at 3 km resolution have been omitted from the scatterplots in **(b)** and **(c)** for clarity, because 23 of 25 3 km retrievals yielded QF = 3 and the remaining two yielded QF = 0.

ACPD
13, 15007–15059, 2013

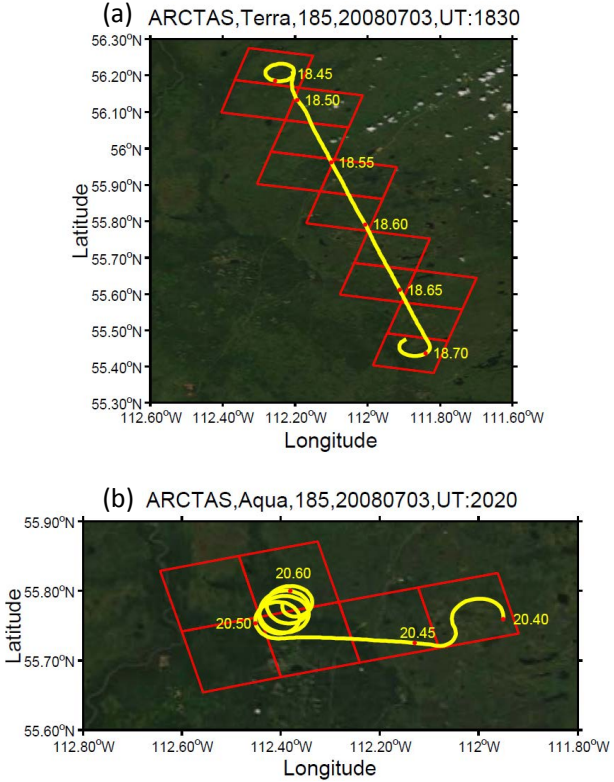

Fig. 8. Overlays of MODIS RGB image with 10 km retrieval grid cell and P-3 flight track locations for **(a)** Terra overpass at 18.5 UT and **(b)** Aqua overpass at 20.3 UT on 3 July 2008.

ACPD
13, 15007–15059, 2013

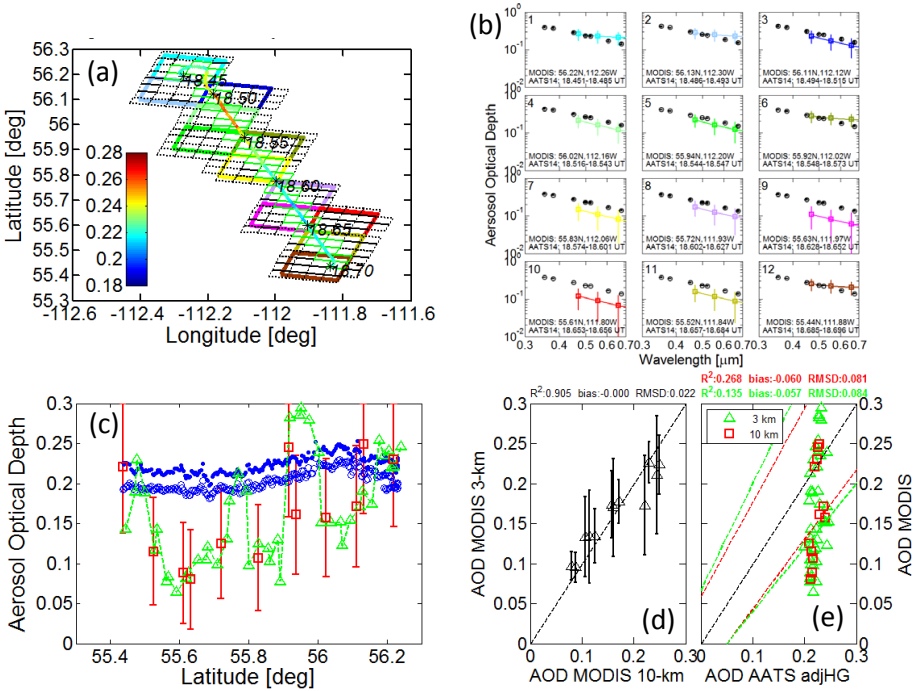

Fig. 9. Multiframe figure for 3 July Terra MODIS/AATS AOD comparison. Figure is analogous to Fig. 3, except MODIS 10 km grid cells in 9 **(a)** have been color-coded to match the MODIS AOD spectra shown in **(b)**, and MODIS spectra are shown only for the operational MODIS retrieval.

ACPD
13, 15007–15059, 2013

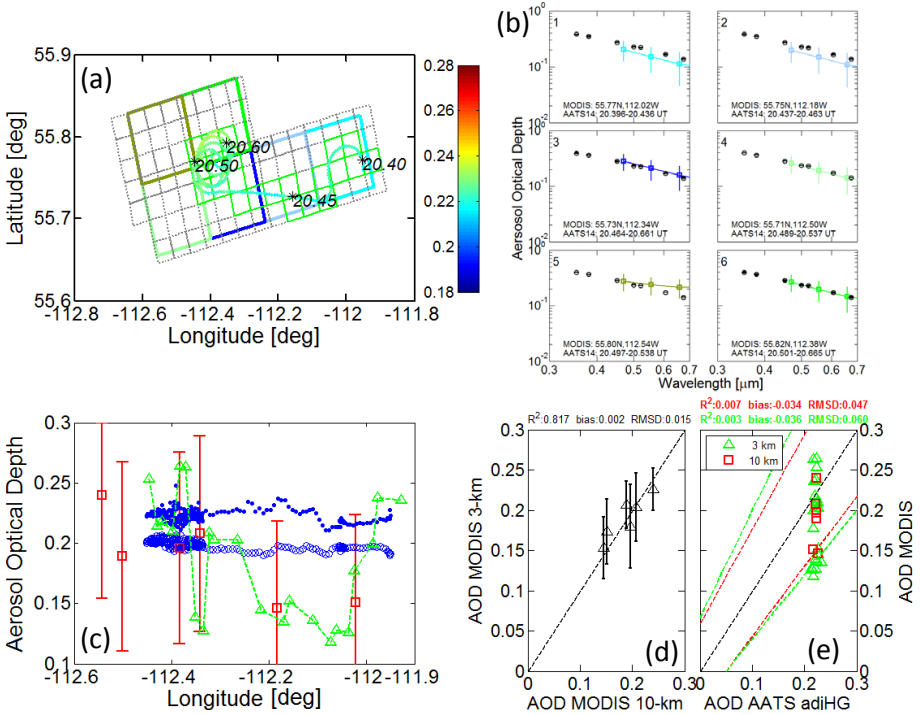

Fig. 10. Same as Fig. 9, but for the 3 July Aqua MODIS/AATS AOD comparison.

ACPD
13, 15007–15059, 2013

Comparison of MODIS 3 km and 10 km resolution

J. M. Livingston et al.

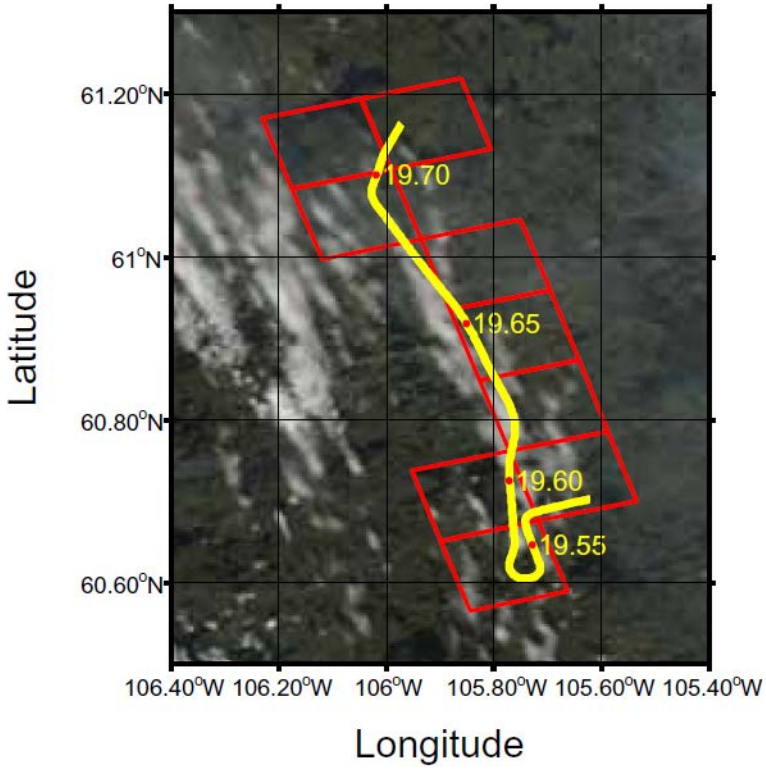

Fig. 11. Overlay of MODIS RGB image with 10 km retrieval grid cell and P-3 flight track locations for Aqua overpass at 19.75 UT on 9 July 2008.

ACPD
13, 15007–15059, 2013

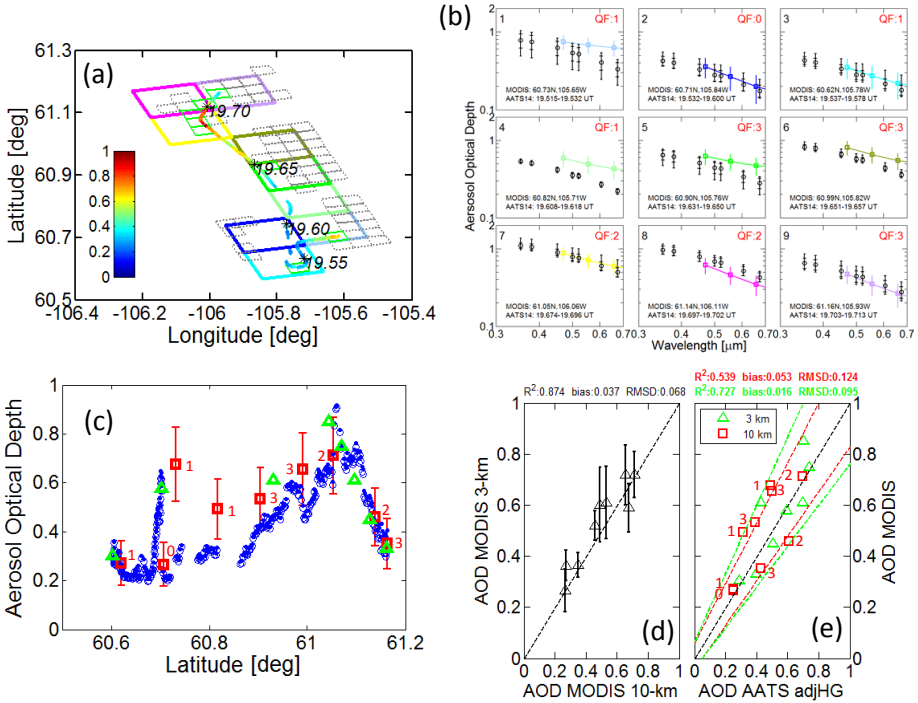

Fig. 12. Analogous to Figs. 9 and 10, but for the 9 July Aqua MODIS/AATS AOD comparison. MODIS retrieval quality flags are listed in red in **(b)**, **(c)**, and **(e)**.

ACPD
13, 15007–15059, 2013

Comparison of MODIS 3 km and 10 km resolution

J. M. Livingston et al.

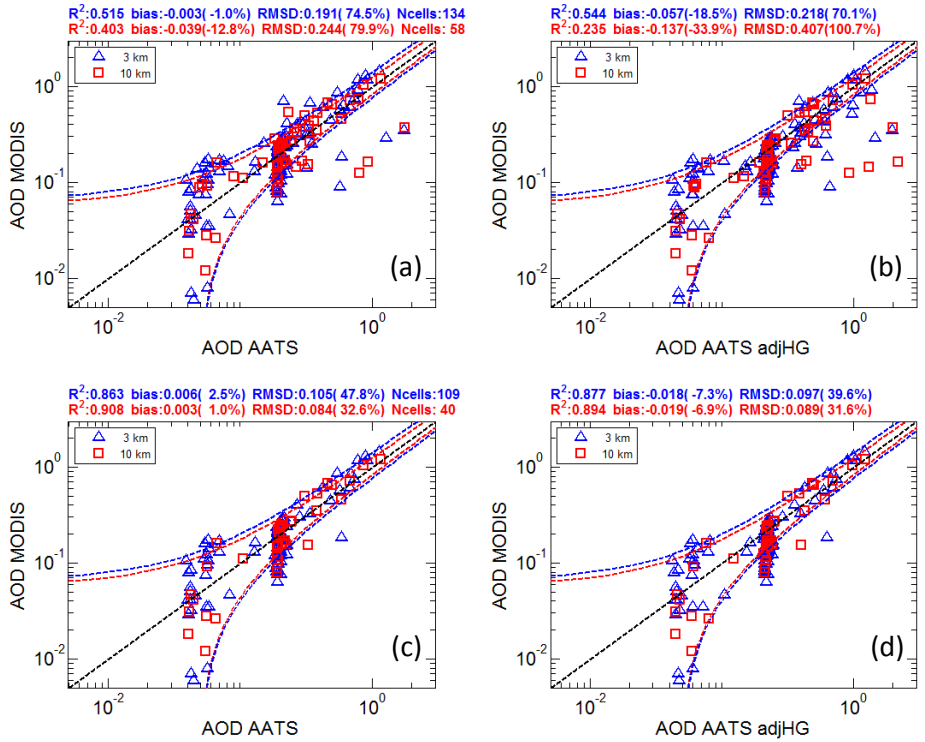

Fig. 13. Scatterplots of MODIS versus AATS AOD for the composite data set. **(a, c)** Results as a function of AATS AOD without the addition of below-aircraft AOD estimates. **(b, d)** Results as a function of AATS AOD with the addition of below-aircraft AOD estimates. Frames **(a, b)** include all 5 cases; frames **(c, d)** omit the 2 July case.

ACPD
13, 15007–15059, 2013

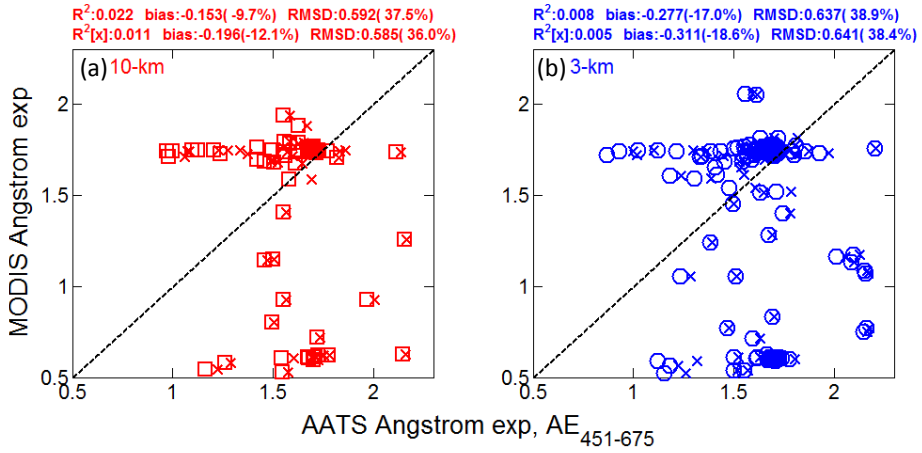

Fig. 14. Scatterplots of calculated MODIS versus AATS AE for the composite data sets for MODIS retrievals at **(a)** 10 km and **(b)** 3 km resolution. Open symbols give the results for AATS values that do not include below-aircraft AOD estimates, and x symbols give the corresponding results for AATS values that do include below-aircraft AOD estimates.

ACPD
13, 15007–15059, 2013